

Ultrathin Broadband Metasurface Superabsorbers from a van der Waals Semimetal

Adam D. Alfieri¹, Michael J. Motala², Michael Snure³, Jason Lynch¹, Pawan Kumar^{1,4}, Huiqin Zhang¹, Susanna Post⁵, Christopher Muratore⁵, Joshua R. Hendrickson³, Nicholas R. Glavin^{*6}, Deep Jariwala^{*1}.

¹Department of Electrical and Systems Engineering, University of Pennsylvania, Philadelphia, PA 19104, USA

²UES Inc. Dayton, OH, 45432

³Air Force Research Laboratory, Sensors Directorate, Wright-Patterson Air Force Base, OH, 45433, USA

⁴Department of Materials Science and Engineering, University of Pennsylvania, Philadelphia, PA 19104, USA

⁵Department of Chemical and Materials Engineering, University of Dayton, Dayton, OH, 45469, USA

⁶Air Force Research Laboratory, Materials and Manufacturing Directorate, Wright-Patterson Air Force Base, OH, 45433, USA

*Corresponding Authors: dmj@seas.upenn.edu; nicholas.glavin.1@afrl.af.mil

Abstract

Metamaterials and metasurfaces operating in the visible and near-infrared (NIR) offer a promising route towards next-generation photodetectors and devices for solar energy harvesting. While numerous metamaterials and metasurfaces using metals and semiconductors have been demonstrated, semimetals-based metasurfaces in the vis-NIR range are notably missing. Here, we experimentally demonstrate a broadband metasurface superabsorber based on large area, semimetallic, van der Waals PtSe₂ thin films in agreement with electromagnetic simulations. Our results show that PtSe₂ is an ultrathin and scalable semimetal that concurrently possesses high index and high extinction across the vis-NIR range. Consequently, the thin-film PtSe₂ on a reflector separated by a dielectric spacer can absorb > 85 % for the unpatterned case and ~97 % for the optimized 2D metasurface in the 400-900 nm range making it one of the strongest and thinnest broadband perfect absorbers to date. Our results present a scalable approach to photodetection and solar energy harvesting, demonstrating the practical utility of high index, high extinction semimetals for nanoscale optics.

1. Introduction

Optical metamaterials and their planar counterpart, metasurfaces, are artificial materials engineered using subwavelength features to exhibit a desired response to electromagnetic fields unachievable with natural materials^[1,2]. Metamaterial perfect absorbers (MMPAs) have been designed for frequencies ranging from the visible to microwave^[3]. Narrow bandwidth MMPAs are typically based on a frequency-dependent resonant response and have applications in spectral filtering^[4] and sensing^[5]. In the visible to near infrared (NIR), broadband MMPAs are important for photodetection and solar energy harvesting^[6,7].

Broadband solar absorption has been achieved using anti-reflectance effects in superlattices of dielectrics and lossy metals^[8], nanostructuring the surface of thick semiconductor wafers^[9], light trapping in vertically aligned nanowire or nanotube arrays^[10-13], and by light trapping in metamaterials with tapered geometries.^[14,15] While effective, these approaches require relatively thick structures and/or complicated fabrication processes, limiting their practicality. Additionally, it is desirable for certain applications—such as photocatalysis—to localize EM waves at or near the surface^[7]. Ultrathin metasurfaces exhibiting near-unity absorption and deep subwavelength field

confinement are therefore ideal as electromagnetic energy is concentrated at the surface while the thin structure enables lightweight, low-cost devices.

A common approach to metasurface absorbers is using a patterned metal film on top of a lossless dielectric spacer layer on a metal reflector^[5,6,16,17]. The dielectric layer recirculates light or can be chosen to produce a Fabry-Perot cavity resonance^[4]. Periodic patterning of the top metal layer results in localized surface plasmon (LSP) modes excited in the top layer^[18] and a gap surface plasmon (GSP) between the two metal films^[19]. These plasmons – collective excitations of electrons at the interface between a metal and dielectric – enhance light absorption/emission and can localize electromagnetic fields to deep subwavelength mode volumes^[18,20]. Further, hot electrons created by plasmons are particularly useful for photoelectrocatalysis^[21], photodetection^[22,23], and plasmonic solar cells^[24].

The periodically patterned metal film exhibits a plasmonic response that is highly dependent on the structure geometry and the polarization and incident angle of the incident light. Moreover, plasmonic responses tend to be narrowband^[6,25] and do not absorb off-resonance light or transverse electric (TE) modes. The polarization dependence can be significantly reduced by patterning elaborate nanoantenna structures^[26,27], and broadband absorption can be achieved by resonance multiplexing^[6,16,28,29] or by incorporating epsilon-near-zero materials in the dielectric spacer^[30]. However, achieving polarization independent broadband absorption in purely plasmonic absorbers requires intricate geometries that make design and fabrication challenging. Using lossy plasmonic metals like chromium, titanium nitride, and tungsten has been shown to improve broadband absorption^[31–38], but the ohmic loss results in energy being dissipated as heat, limiting potential applications.

Alternatively, two-dimensional metal dichalcogenides exhibit strong interaction with light despite ultrathin thicknesses^[39–41]. Among them, noble metal dichalcogenides (NMDs) of form MX_2 ($\text{M} = \text{Pt}, \text{Pd}; \text{X} = \text{S}, \text{Se}, \text{Te}$) have only been recently explored^[42–49]. PtSe_2 is an indirect-gap semiconductor in the monolayer limit but becomes a type-II Dirac semimetal beyond a few layers in thickness^[50–52]. PtSe_2 has attracted the attention of researchers due to its broadband optical properties^[53,54], saturable absorption^[55], air stability^[47], low temperature synthesis compatible with CMOS back end of line (BEOL) processing^[56], and high mobilities in single crystalline flakes and films^[57]. Additionally, PtSe_2 has demonstrated immense promise as a photo-electrocatalytic material^[44,58–63]. Broadband absorption and strong catalytic properties make PtSe_2 an exciting material for broadband metasurface solar absorbers with direct applications in solar photocatalysis.

In this work, we demonstrate the scalable synthesis of PtSe_2 thin films with extraordinarily large refractive index and extinction, dominated by inter-band optical transitions, throughout the visible-NIR range. We then replace the commonly used top metal film in the metal-insulator-metal (MIM) metasurface structure with a semimetallic PtSe_2 film. We show that use of the dielectric spacer and back reflector are sufficient to achieve broadband absorption even in unpatterned films. By patterning the PtSe_2 to produce plasmons from the Ag and dielectric modes in the PtSe_2 , broadband near unity absorption (97.0 %) is achieved from 400 nm to 900 nm. Remarkably, our PtSe_2 -based approach stands out as simultaneously among the strongest and thinnest broadband thin-film or meta-absorbers known to date, exemplifying the broader value of taking a materials-first approach

to nanophotonics: simple designs with emerging high-index materials can outperform more complex designs using conventional materials.

2. Results and Discussion

2.1. Synthesis and Characterization

PtSe₂ films were synthesized via thermally assisted conversion (TAC) of a sputtered Pt film^[56,64] by annealing in H₂Se at 550°C (see Methods). A picture of a large area PtSe₂ grown by TAC on sapphire is shown in Figure 1a. Raman spectra (Figure 1b) collected at 5 spots on the sample, corresponding to locations at the center and at each edge, confirm the formation of PtSe₂ with high uniformity across the sample. The peaks observed at 178 cm⁻¹, 206 cm⁻¹, and ~237 cm⁻¹ correspond to the E_g, A_{1g}, and longitudinal optical (LO) modes of PtSe₂^[65]. Cross-sectional transmission electron micrographs confirm the horizontally aligned, well-layered structure, and high angle annular dark field (HAADF) elemental mapping verifies the complete selenization of the film (supporting information section S1.1.). We synthesized PtSe₂ at temperatures ranging from 375°C to 650°C (supporting information section S1.1.) and found that annealing at 550°C produced films with the largest optical constants (supporting information section S1.2.1.), but the ability to selenize PtSe₂ at 450°C and lower makes this process CMOS BEOL compatible^[64,66]. The large area films can then be transferred to arbitrary substrates using the well-established PMMA-assisted wet transfer process (Methods).

We determined the complex refractive index (Figure 1c) of 17 nm PtSe₂ transferred onto 40 nm Al₂O₃/100 nm Ag/300 nm SiO₂/Si by spectroscopic ellipsometry and fitting using Lorentzian oscillators (Methods and supporting information section S1.2.1.). In the complex refractive index, $\eta = n + ik$, k is directly related to absorptivity/extinction while n is related to propagation and power localization. The optical response of PtSe₂ in the UV/vis regime is dominated by a high density of interband transitions between Se- p and Pt- d bands near the Fermi level^[67], resulting in a large, broadband k . The massive n and k in the vis-NIR result in strong broadband absorption. The semimetallic optical behavior of PtSe₂ is seen by examining the optical constants: at approximately 470 nm, where the n and k intersect, consistent with prior works^[53,54]. Below this critical point, the real part of the relative permittivity ($\text{Re}(\epsilon) = n^2 - k^2$) is negative, so the optical properties of PtSe₂ are more metallic, but the Lorentzian oscillator terms and lack of a Drude term in the optical fitting indicate that the optical properties are still dominated by interband transitions and not free carrier behavior. $\text{Re}(\epsilon)$ is positive from 470 nm to 900 nm, so PtSe₂ behaves like a semiconductor or lossy dielectric in this range.

The extraordinary broadband optical properties of PtSe₂ are evident upon transfer from the growth substrate (sapphire wafers) onto a silver mirror coated with 40 nm Al₂O₃ (Figure 1d, inset), resulting in >85% absorption in the unpatterned case (Figure 1d). Broadband >85% absorption in a 17 nm thick semimetallic film using only a back reflector and a lossless dielectric to recirculate light is remarkable, particularly because it presents a scalable lithography-free approach to broadband light-harvesting in ultra-thin geometries. For the remainder of this study, we explore the enhancement of the optical absorption of this 3-layer structure to near unity by exploiting the PtSe₂ absorption and the plasmonic properties of silver.

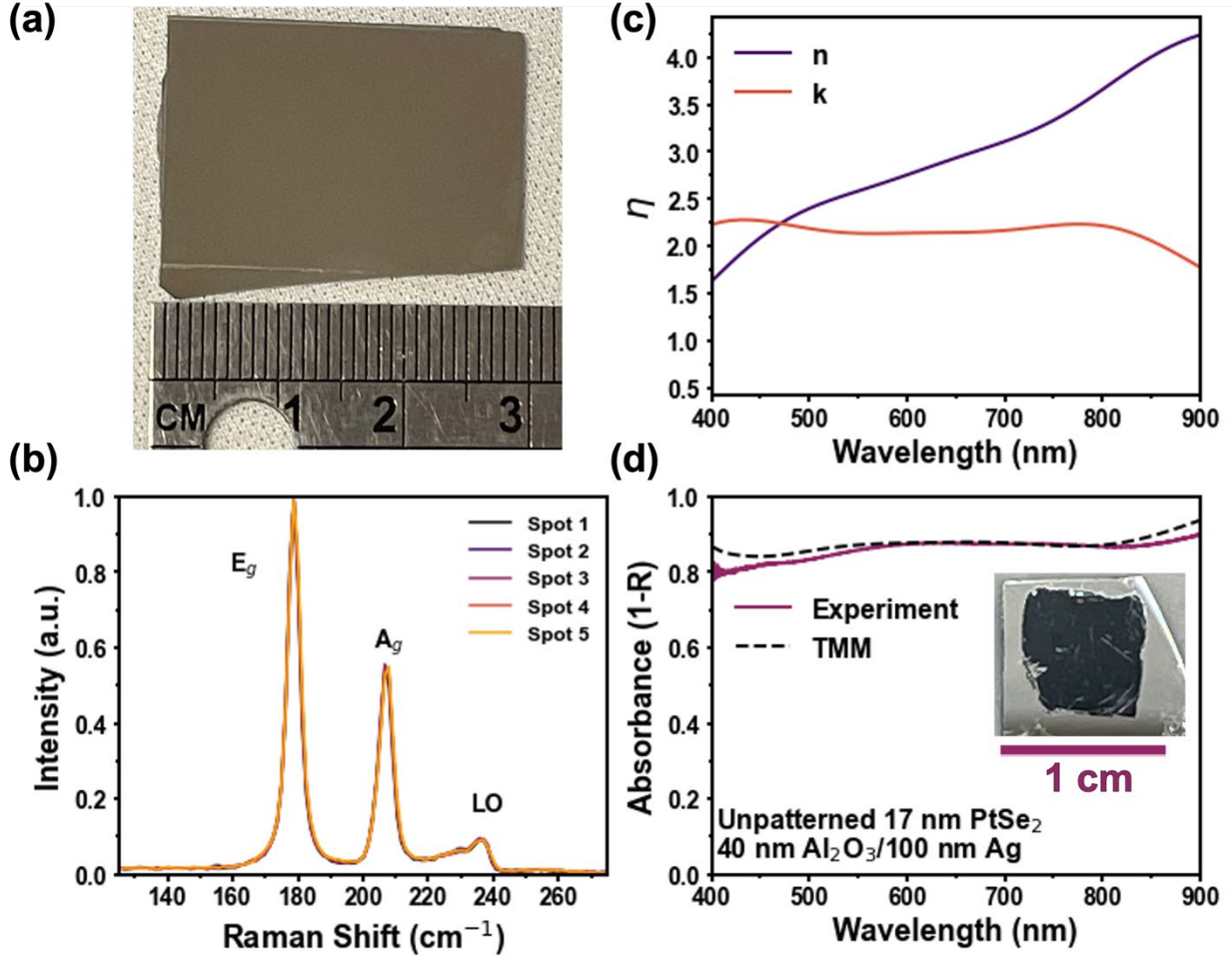


Figure 1. PtSe₂ Film Structural and Optical Characterization. (a.) A large area PtSe₂ film as grown on sapphire (b.) Raman characterization of a PtSe₂ film as grown on sapphire, taken at 5 different spots that are randomly and evenly distributed across the film. (c) Real and imaginary parts of the refractive index: $\eta = n + ik$. (d) Experimental and transfer matrix method (TMM) calculated absorbance spectra of an unpatterned PtSe₂ film transferred onto 40 nm Al₂O₃/100 nm Ag/SiO₂/Si. Inset: a picture of the sample. Optical constants for PtSe₂ were determined by spectroscopic ellipsometry on a transferred film.

2.2. Nanoribbon Array Metasurfaces

The first structure considered for broadband absorption is a 1D metasurface based on nanoribbons patterned in the 17 nm thick PtSe₂ film by a combination of electron beam lithography and reactive ion etching (further details found in Methods). In this structure, the top metal layer of the common MIM metasurface is replaced with PtSe₂. While PtSe₂ does not exhibit a LSP resonance, it is highly absorptive. Moreover, nanopatterning of the PtSe₂ still excites plasmons^[68] and results in GSP-like modes. Figure 2a shows a schematic of the 3-layer structure: the top layer is composed of PtSe₂ nanoribbons with width w , arranged in an array with period p ; the middle layer is a 40 nm thick Al₂O₃ film; and the bottom layer is a sputtered 100 nm thick Ag film. The substrate is Si with a 300 nm thick thermal oxide. There is no transmission through the Ag mirror, so the substrate choice is arbitrary as long as it is flat and smooth. Because there is no transmission, we can approximate the absorption of films and metasurfaces from the reflectance spectra as $A \approx 1 - R$. This is not exact, as there will be some scattering due to surface roughness.

We fabricated nanoribbon arrays with a fixed period $p = 300$ nm and widths varying from 110 nm to 225 nm by patterning 15×15 micron pixels in PtSe₂ (Figure 2b and Figure 2c). The pixels look increasingly dark with increasing width, and the higher fill factor arrays look darker than the unpatterned PtSe₂, which itself absorbs over 85% of visible light. The unpolarized reflectance measurements in Figure 2d confirm the absorbance broadening with increasing nanoribbon fill factor. By patterning the PtSe₂ into a 1D metasurface, the absorption can be enhanced relative to the unpatterned film across the broadband spectral region between 400 nm and 900 nm.

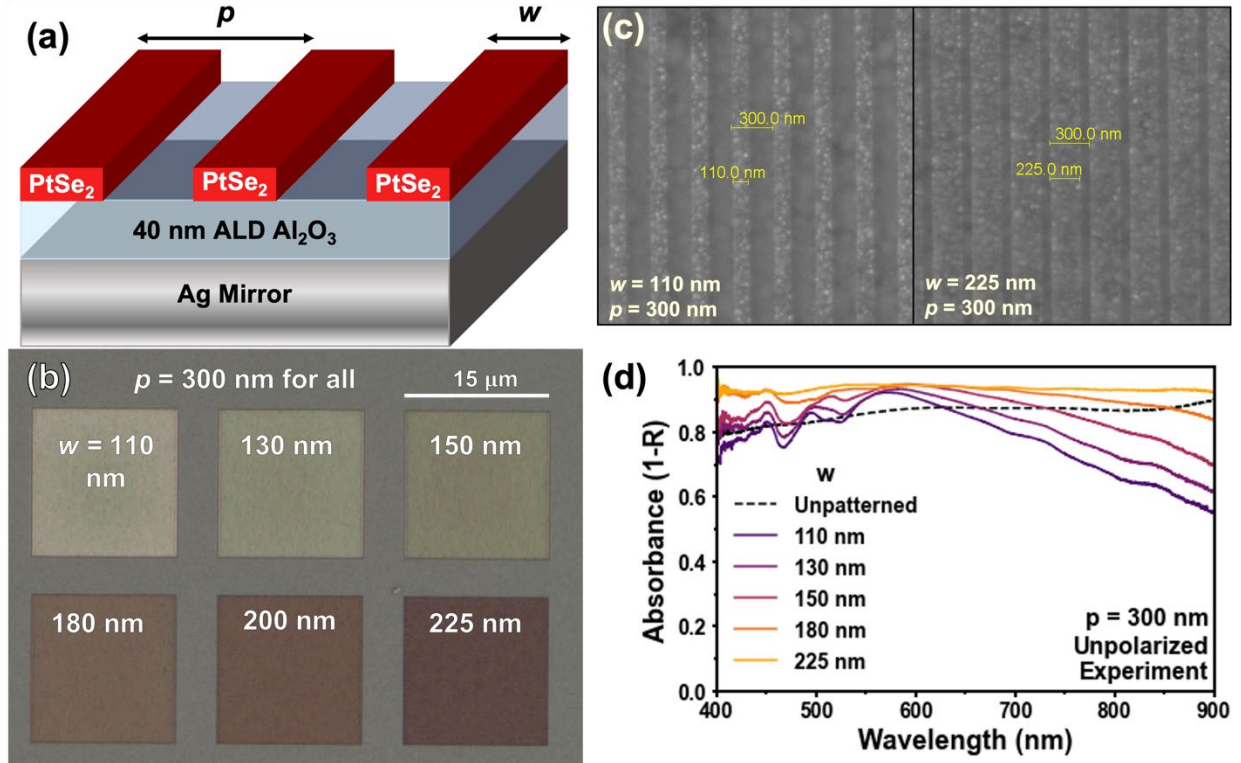


Figure 2. PtSe₂ Nanoribbon Array Structure and Unpolarized Reflectance. (a) Schematic of a PtSe₂ nanoribbon array. The nanoribbons sit on a 40 nm Al₂O₃ layer on a 100 nm Ag mirror. The nanoribbons have width w and are arranged in a 1D array with period p . (b) Unpolarized optical image of a set of array pixels with widths ranging from $w = 110$ nm to 225 nm. All arrays have period $p = 300$ nm. The area surrounding the $15 \mu\text{m} \times 15 \mu\text{m}$ pixels is the unpatterned PtSe₂ film. (c) Scanning electron microscope images of arrays with $w = 110$ nm (left) and $w = 225$ nm (right). Both structures have period $p = 300$ nm. Measurements using the SEM software overlaid on the images confirms the accuracy of the patterning. (d) Unpolarized absorbance spectra for the arrays shown in (b) and the unpatterned film area.

The absorption mechanisms can be better understood by considering separately the transverse electric (TE) and transverse magnetic TM polarized modes of the nanoribbon array. At normal incidence, we define TE polarized light as linearly polarized plane waves with the electric field component parallel to the nanoribbon length while TM polarized light has its electric field component orthogonal to the nanoribbon length, respectively.

2.2.1. Transverse Magnetic Modes of PtSe₂ Nanoribbons

For normal incidence TM polarized light, the in-plane wavevector depends only on the array period:

$$k_x(\theta = 0) = 2\pi m/p \quad m = \text{integer} \quad (1)$$

The nonzero k_x excites plasmons from the Ag film and results in an enhanced electric field in and around the nanoribbons. To characterize the plasmonic response, we first consider arrays with constant fill factor, $f = w/p \approx 1/3$. Figure 3a is a TM-polarized optical image of a die with various pixels corresponding to different nanoribbon periods ranging from 150 nm to 1500 nm, all with w approximately $p/3$. Structural color changing with period is a clear signature of a visible range plasmonic response. We characterize the plasmon resonances by performing normal-incidence reflectance spectroscopy with TM light (Figure 3b) on the arrays shown in Figure 3a for periods 150 nm to 360 nm. The spectra with increasing period are vertically offset by 0.5 to better visualize the shift of the plasmon resonances, which are taken to be reflectance minima in the spectra.

There are 3 different resonances in the experimental spectra: a lower energy plasmon and a higher energy plasmon – denoted P1 and P2 for brevity – and a waveguide mode that appears in the experimental spectra due to imperfect collimation of the incident beam, resulting in a slight incident angle that causes the peak seen in the simulated spectra to split (supporting information S2.2.3.). Both the P1 and P2 modes are well predicted by simulation. The profiles of the P1 and P2 modes, the effects of the dielectric layer material on the TM modes, and the effects of dielectric layer thickness on the TM modes are further discussed in supporting information section S2.2.

Figure 3c shows the electric field magnitude and power absorbed (P_{abs}) profiles for the nanoribbon array structures (seen in Figure 2b) with $p = 300$ nm and $w = 225$ nm under normal incidence TM illumination with wavelength $\lambda = 550$ nm. The plasmonic response results in electric field enhancement in and around the PtSe₂. Using this simulated field profile, we can directly calculate the power absorbed in each material using the formula for a nonmagnetic material:

$$P_{abs} = \frac{1}{2} \omega \text{Im}(\epsilon) |\mathbf{E}|^2 \quad (2)$$

The P_{abs} profiles for the TM modes of the nanoribbon structure are enhanced at the center of the PtSe₂ where the electric field is localized. Based on control simulations (supporting information section S2.2.2.) and the relatively small amount of power absorbed in the silver (5.4% on average), we can conclude that the absorption of TM polarized light is almost entirely due to the PtSe₂ interband absorption. Moreover, the absorption is at a maximum where the field is enhanced by plasmons, so it is clear that the field localization and enhancement by the plasmonic resonance assist absorption.

In Figure 2d, the absorption spectra increase and slightly redshift with increased w for a fixed p of 300 nm. This trend is observed for TM polarized light in experiment (Figure 3d, left) and simulation (right): the plasmon resonances redshift and broaden with increasing fill factor. The broadening of the resonance and enhancement of the absorption are both enabled by the large extinction of the PtSe₂ (supporting information section S2.2.4). The P1 and P2 modes are distinguishable for lower fill factor structures, and each broaden out into a broadband absorbance spectrum with no distinguishable modes as the fill factor increases. The waveguide mode again appears in the experimental spectrum at approximately 510 nm and redshifts slightly with increasing fill factor. The main phenomena of interest– resonance broadening and absorption enhancement– are well predicted by the simulations.

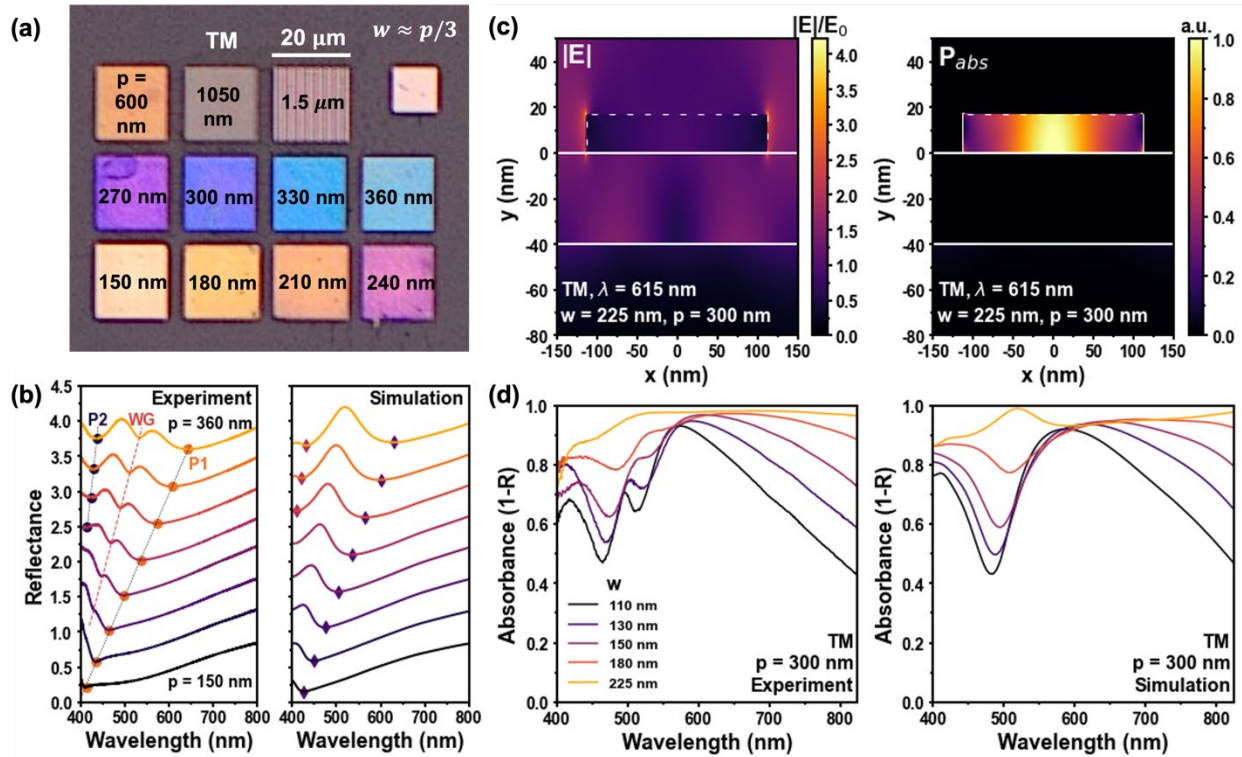


Figure 3. Nanoribbon Array Transverse Magnetic Modes and Absorption. (a) A TM-polarized optical image of nanoribbon array pixels with an approximate fill factor of $1/3$ and periods ranging from 150 nm to 1500 nm. The area surrounding the pixels is the unpatterned PtSe_2 film. (b) Experimentally measured (left) and simulated (right) reflectance spectra for the arrays shown in (a) with p ranging from 150 nm to 360 nm in 30 nm increments. Spectra are vertically offset by 0.5 for clarity. The P1, P2, and waveguide (WG) modes are labeled on the experimental spectra, and dotted lines are added to guide the eye. The plasmon resonances on both the experimental and simulated spectra are indicated with dots (experiment) and diamonds (simulation). (c) Electric field magnitude (left) and power absorption (right) profiles for a nanoribbon array ($w = 225$ nm, $p = 300$ nm) illuminated by a TM wave ($\lambda = 615$ nm). (d) Experimentally measured (left) and simulated (right) TM-polarized absorbance spectra (taken to be $A = 1 - R$) for the arrays shown in Figure 2b with $p = 300$ nm and w ranging from 110 nm to 225 nm. The linearly polarized data in (d) extends only up to 825 nm due to the limited bandwidth of the linear polarizer.

2.2.2. Broadband Absorption of TE Polarized Light in PtSe_2 Nanoribbons

In addition to strong plasmon-enhanced absorption, the PtSe_2 nanoribbons exhibit broadband absorption for TE light. Figure 4a shows the experimental (top) and simulated (bottom) TE-polarized absorbance spectra for the structures in Figure 2b with a fixed $p = 300$ nm and varying widths. Like the plot for the TM case, the polarized data is limited from 400 nm to 825 nm by the polarizer bandwidth. The experimental spectra match up well with the corresponding simulated spectra for most of the measured area. Even for TE polarizations, the absorbance is enhanced relative to the unpatterned case for part or all of the measured range, depending on the array dimensions. Here we see the benefit of replacing the top metal layer in a MIM broadband metasurface absorber with a high index, high- k material: there is strong absorption even for polarizations that do not excite the plasmon resonance.

Enhanced absorption despite removal of absorbing material indicates that patterning PtSe₂ results in the excitation of lossy modes due to the PtSe₂ itself, given the lack of a plasmon resonance for TE polarizations. Figure 4b shows the TE $|E|$ field profiles and the P_{abs} profiles for a nanoribbon array with $w = 225$ nm, $p = 300$ nm at wavelengths of 405 nm and 825 nm, respectively. The P_{abs} profiles are normalized to the maximum value of P_{abs} across both wavelengths and are not a measure of the fraction of the incoming power absorbed. On average, the P_{abs} in the Ag mirror is only 1.7%. Control simulations further confirm that the absorption is due to the large k of PtSe₂ (supporting information S2.2.5.). For $\lambda = 405$ nm, the electric field is enhanced between the ribbons; we expect that this is due to the $\text{Re}(\epsilon) < 0$ of PtSe₂ below 470 nm. The corresponding P_{abs} profile shows that power absorption primarily occurs towards the edges of the ribbons. In the spectra shown in Figure 4a, the absorption maximum below 470 nm increases and blue shifts slightly with increasing fill factor as the field is being confined in a narrower area before decreasing for $w = 225$ nm. In contrast, the electric field and power absorption are more concentrated in the center of the ribbons for $\lambda = 825$ nm, indicating dielectric confinement due to the large n of PtSe₂. At intermediate wavelengths where the material behaves like a lossy dielectric (between 470 nm and 825 nm), we expect that the absorption is also enhanced due to localization of light in the high-index nanoribbons. Overall, dependence of absorbance on fill factor is less drastic than for the TM case, and broadband absorption is seen for all ribbon widths.

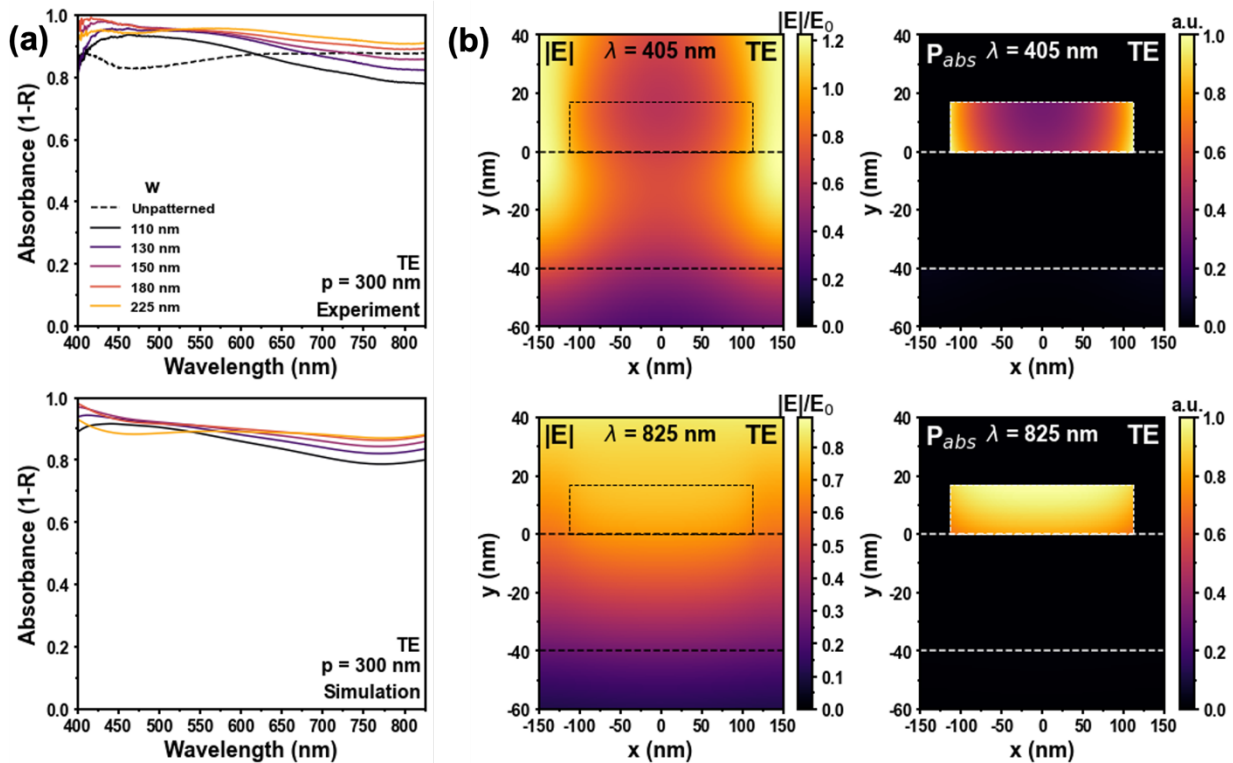


Figure 4. Nanoribbon Array Transverse Electric Absorption. (a) Experimentally measured (top) and simulated (bottom) transverse electric (TE)-polarized absorbance spectra for the arrays shown in Figure 2b with $p = 300$ nm and w ranging from 110 nm to 225 nm. The experimental data (b) $|E|$ field (left) and corresponding P_{abs} (right) profiles for a nanoribbon array ($w = 225$ nm, $p = 300$ nm) illuminated with TE-polarized plane waves of wavelength $\lambda = 405$ nm (top) and $\lambda = 825$ nm (bottom). The P_{abs} profiles are normalized to the maximum value of P_{abs} to provide a relative comparison.

2.3. 2D Array PtSe₂ Metasurfaces

Now that we have observed the contributions to absorption of the Ag and PtSe₂ in a 1D nanoribbon array structures, we design relatively simple 2D arrays to maximize absorption of unpolarized visible light. We maintain the general 3-layer structure of PtSe₂ transferred on 40 nm Al₂O₃/100 nm Ag, but now fabricate 2D arrays. 2D periodicity results in nonzero in-plane wavevectors in both the \hat{x} and \hat{y} directions, exciting plasmon polaritons for all polarizations. For any given polarization, we expect the simultaneous presence of TM-like absorption modes – for which the Ag plasmons assist absorption by localizing the electric field in and around the PtSe₂ – and TE-like lossy dielectric modes due to the strong n and k of PtSe₂. Absorber design is therefore flexible and can be tailored to applications as any well-designed periodic, high PtSe₂ fill factor pattern will exhibit broadband near-unity absorption. We demonstrate this by fabricating structures with simple, inverted patterns: crossed PtSe₂ gratings/nanoribbons (XGs, Figure 5a - top) and a square array of PtSe₂ nanosquares (NSQs, Figure 5a - bottom). The XGs can alternatively be thought of as a square array of square nanoholes. The calculated field profiles and power absorption profiles are discussed in detail in Supporting Information section S3.2. The absorption of the XGs is more similar to the TE response of the nanoribbons, i.e., field localization and absorption are largely due to the large refractive index. In contrast, absorption in NSQ arrays is dominated by plasmonic field enhancement in the PtSe₂, similar to the TM modes of the nanoribbon arrays.

Dies were fabricated with 3 XGs and 3 NSQ arrays per die. SEM images of representative structures are shown in Figure 5b. The XGs have a fixed $p = 300$ nm and different w 's of 100 nm, 150 nm, and 200 nm, respectively. The NSQ arrays have the following dimensions (w, p): (150 nm, 200 nm), (150 nm, 300 nm), (250 nm, 300 nm). Figure 5c is an unpolarized optical image of a die of metasurface pixels. We see that all pixels – except for NSQ (150 nm, 300 nm) – look dark or even completely black compared to the unpatterned PtSe₂ film, which itself absorbs over 85% of visible light. Unpolarized reflectance measurements (Figure 5d) show broadband near-unity absorption for all metasurfaces except the array of 150 nm NSQs with period 300 nm. We note that the XGs exhibit less dependence on fill factor than the NSQ arrays over the range of dimensions considered. This is well predicted by FDTD simulation of the structures with a broadband plane wave polarized along the \hat{x} direction (supporting information section S3.3.).

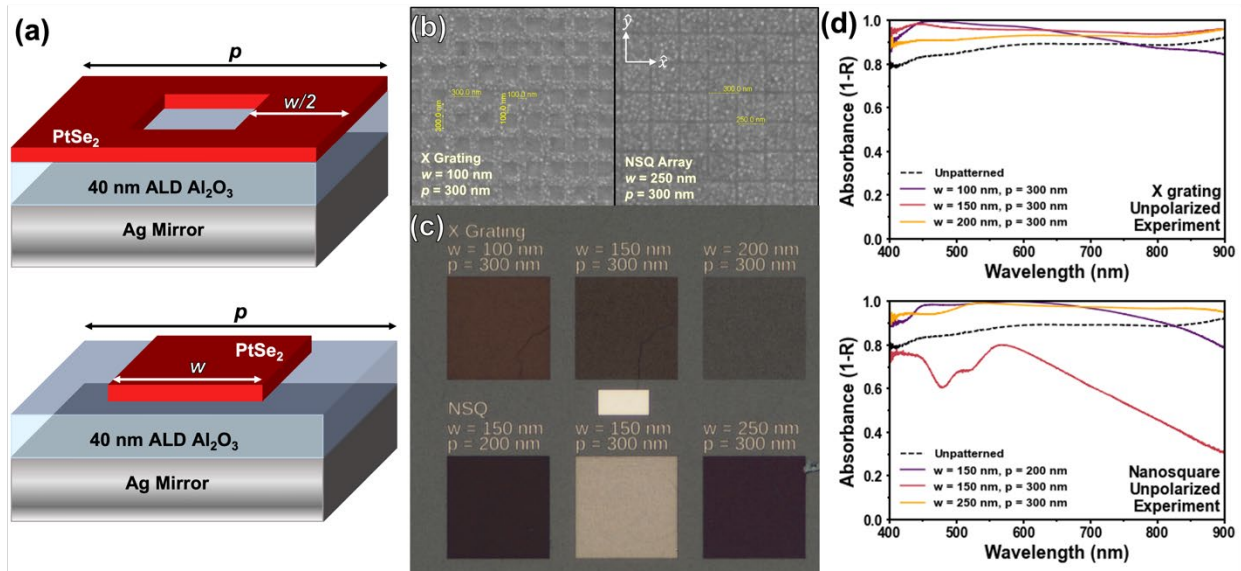


Figure 5. 2D Array PtSe₂ Broadband Metasurface Superabsorber Structures and Experimental Results. (a) Schematics of single unit cells of the crossed grating (XG) metasurface (top) and the nanosquare (NSQ) metasurface (bottom). (b) Scanning electron microscope (SEM) images of an XG metasurface (left) with dimensions $w = 100$ nm and $p = 300$ nm and NSQ array metasurface (right) with dimensions $w = 250$ nm and $p = 300$ nm. Measurements of the feature sizes using SEM software are displayed on the images, confirming accurate dimensions. (c) Unpolarized optical micrograph of a representative die, consisting of six $20 \mu\text{m}$ by $20 \mu\text{m}$ pixels patterned into PtSe₂ – the metasurfaces – and a small white rectangular patch where the PtSe₂ is removed to show the alumina-coated Ag substrate. The top row of pixels is a set of XGs while the bottom row is a set of NSQ arrays. The structure dimensions for each pixel are lithographically patterned into the PtSe₂ film. (d) Absorbance spectra of XGs (top) and NSQ arrays (bottom) as determined by normal incidence unpolarized reflectance spectroscopy. The unpatterned PtSe₂ film absorbance spectrum is included for reference. All reflectance data is normalized to a baseline spectrum from substrate and corrected for background noise (methods).

The integrated absorbance of all light in the visible range (400 nm to 700 nm), A_{vis} , and the integrated solar absorption efficiency, A_{solar} , over the measured range (400 nm to 900 nm) are calculated and tabulated (Table 1) as follows:

$$A_{vis} = \frac{1}{300 \text{ nm}} \int_{400 \text{ nm}}^{700 \text{ nm}} A(\lambda) d\lambda \quad (3a)$$

$$A_{solar} = \frac{\int_{400 \text{ nm}}^{900 \text{ nm}} A(\lambda) P_{solar}(\lambda) d\lambda}{\int_{400 \text{ nm}}^{900 \text{ nm}} P_{solar}(\lambda) d\lambda} \quad (3b)$$

$A(\lambda) = 1 - R(\lambda)$ is the measured absorbance spectrum for a given structure (Figure 5d), and $P_{solar}(\lambda)$ is the solar irradiance spectrum (ASTM G-0173-03 1.5AM Standard). The results are plotted in Figure 6 for unpatterned films and selected metasurfaces. Up to 97.9% absorption of visible light and 97.0% absorption of solar light (400 nm to 900 nm) is achieved, enhanced from 86.4% of visible light and 87.6% of solar light for the case of unpatterned PtSe₂ on the dielectric coated silver mirror. We reiterate that the absorption is occurring almost entirely within a 17 nm thick film with < 6% power absorbed on average by the Ag mirror from 400-900 nm. Near unity solar absorption concentrated in a large area, 17 nm strongly photo-catalytic^[44,58–63] layer is therefore a significant step towards solar photocatalysis in this class of materials.

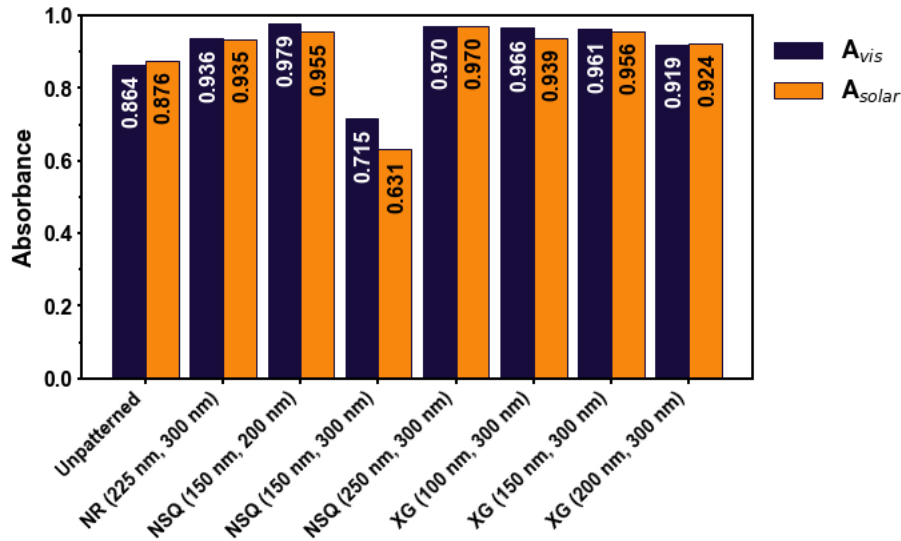


Figure 6. Integrated Visible and Solar Light Absorption for Selected Structures. Integrated visible range absorbance (A_{vis}) and integrated solar absorbance efficiency (A_{sol}) calculated by (3a) and (3b) for unpatterned structures, a selected nanoribbon array (NR) structure, the three different nanosquare array metasurfaces (NSQ), and the three different crossed grating metasurfaces (XG). The dimensions in parentheses are the width and period of the structures, respectively.

We compare the A_{vis} of our best structures for visible range absorption (the NSQ array with $w = 150$ nm, $p = 200$ nm) to other broadband absorbers in literature (Figure 7), plotting A_{vis} as a function of total structure thickness and the thickness of the active layer (i.e., the layer(s) in which most or all light is absorbed). Our PtSe₂-based metasurface stands out as simultaneously among the thinnest and strongest absorbing broadband absorbers to date. To our knowledge, the only experimental study that has demonstrated higher average visible absorption in a total thickness less than 700 nm was Wang *et al.*^[36], which achieved 99.6% average visible absorption in a TiN/AlN nanocomposite active layer (126 nm thick) but required a 100 nm thick anti-reflective coating (ARC). We demonstrate comparable absorption in a thinner overall structure and in a 17 nm thick active layer that is on the surface – i.e., without the need for an ARC. Further, we achieve comparable or greater absorbance as compared to vertical nanowire arrays exceeding 1 micron in thickness^[10,11,13].

Broadband near-unity visible light absorption concentrated in a 17 nm thick PtSe₂ film is noteworthy result due to its potential for both enhanced photodetection and efficient solar photocatalysis in ultrathin, lightweight devices. While some metals are either good absorbers (Ti, Cr, W) or good catalysts for the hydrogen evolution reaction (Pt, Ir, Rh), they are generally not both^[69]. PtSe₂ maintains much of the catalytic activity of Pt but is a significantly more efficient absorber as a Dirac semi-metal. Further, the Pt film precursors are extremely thin, lowering the cost relative to pure Pt electrodes. Additionally, like semiconductors, PtSe₂ perfect absorbers can be applied to photodetection^[70]. However, conventional semiconductors have significantly smaller and more narrowband imaginary refractive indices than PtSe₂ for most of the visible-NIR range^[71] and are otherwise not suitable for efficient light harvesting or photodetection in ultrathin films with high surface-to-volume ratios due to processing difficulties, oxidation, and the effects of surface states on electrical transport and non-radiative recombination. Van der Waals PtSe₂ layers have self-passivated bonds and therefore enable much more practical devices and photocatalysts from ultrathin absorbers.

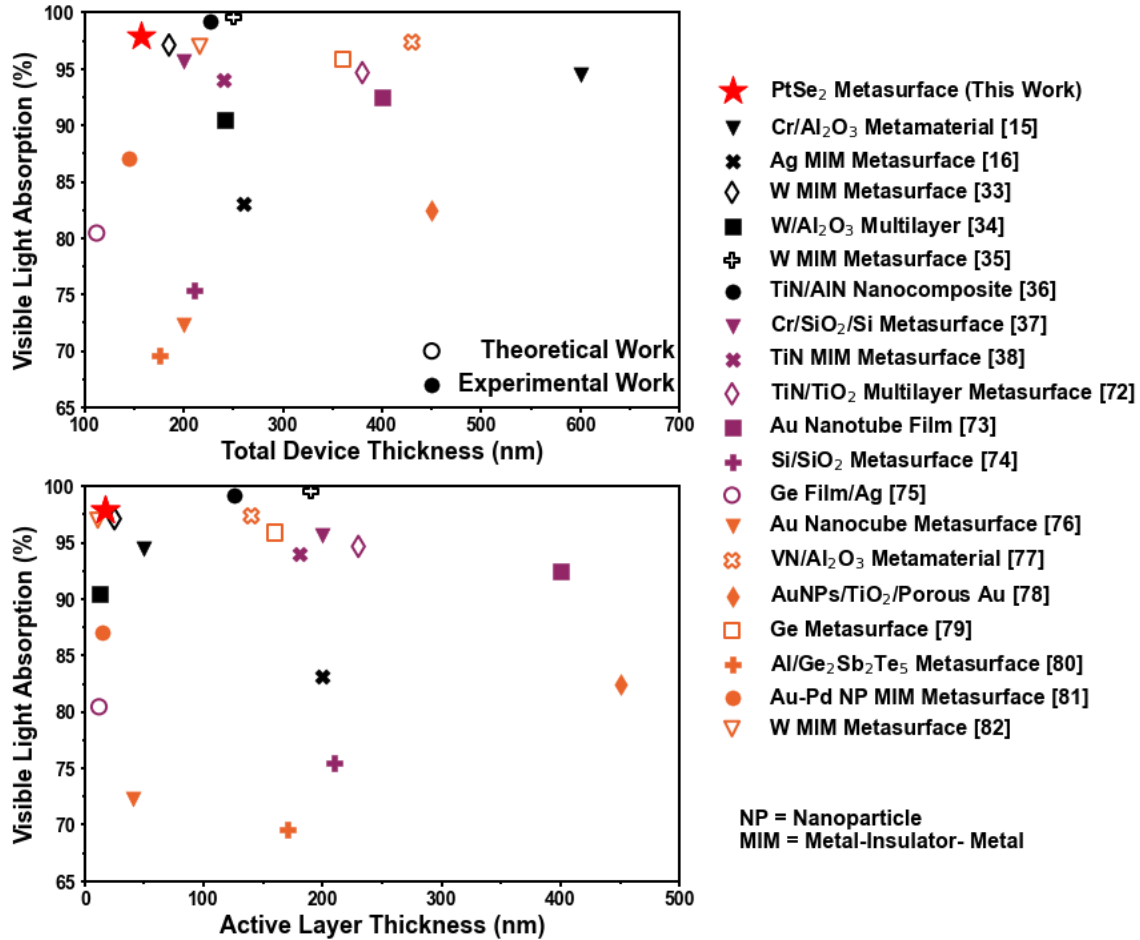


Figure 7. Benchmarking Visible Absorbance of our PtSe₂ Metasurface Against Other Absorbers. Plot of average visible range (400 nm to 700 nm) absorption as a function of total thickness (top) and active layer thickness (bottom) for the PtSe₂ NSQ array metasurface ($w = 150$ nm, $p = 200$ nm; denoted by a red star) and other broadband absorbers demonstrated in literature^[15,16,33–37,72–82]. We define the active layer to be the layer(s) in which most of the power is absorbed. We estimate the absorbance as a function of wavelength for the best result in each previous work at various points from figures in each publication, then estimate the average light absorption using equation (3a). Experimental works are denoted by solid markers while theoretical works are denoted by unfilled markers.

Summary and Outlook

In summary, we have demonstrated the synthesis of 17 nm thick PtSe₂ films with large real and imaginary refractive indices. The large, broadband refractive index and extinction were leveraged to realize strong absorption (> 87 %) in the 400-900 nm range for an ultrathin, cm² scale reflector (Ag)/spacer (alumina)/absorber (PtSe₂) structure in a lithography-free approach. Upon using lithography to pattern the PtSe₂ into 1D and 2D metasurfaces of nanoresonator arrays, broadband absorption was further enhanced to 97% in the most optimized 2D metasurface comprising nanosquare resonators. Finally, all our experimental observations were verified with electromagnetic simulations which suggest that the enhanced broadband absorption in PtSe₂ metasurfaces is a consequence of both: 1. the large optical indices intrinsic to the PtSe₂ due to its semi-metallic character as well as 2. nanophotonic effects such as plasmonic and dielectric resonances. This work pioneers the use of ultrathin PtSe₂-based metasurfaces for broadband visible and near infrared light absorption. Our approach presented here can be generalized to other existing

and to-be-discovered van der Waals semimetallic and semiconducting materials exhibiting high broadband extinction due to interband transitions, presenting an exciting opportunity to design future metasurfaces for photodetection, photochemistry, and solar energy harvesting. We expect that our metasurfaces will be particularly promising for solar photocatalysis given the strong solar absorbance in a catalytically active material, plasmonic field enhancement and hot electron generation.

Methods

PtSe₂ Synthesis

100 mm single-side polished c-plane sapphire substrates (UniversityWafer) were diced with a diamond scribe and subsequently cleaned by sonicating in acetone and isopropyl alcohol before being blow-dried with N₂. Samples were then loaded in a custom-built sputtering system with a minimum base pressure of 3×10^{-8} Torr. A 2" Pt sputter target was mounted on a 2" Mak sputter source (MeiVac, Inc.) and positioned at an angle of 30° and distance of 8 cm from the substrate. A ~ 2 nm thick Pt precursor layer was deposited at room temperature using a Pinnacle Plus pulsed power supply (Advanced Energy) operated at a nominal power of 90W, pulse frequency of 65 kHz, and a pulse width of 0.4 μs under argon with a pressure of 15 mTorr and Ar flow rate of 25 sccm. The total deposition time was 8 seconds.

Formation of PtSe₂ was performed via thermally assisted conversion. The samples were loaded in a tube furnace and held under vacuum for one hour, then pumped under H₂ gas (200 sccm) for another hour. The pressure was then increased to 500 Torr under a flow of 10 sccm H₂ and 160 sccm N₂. The temperature was ramped from room temperature to 550°C over 20 minutes then allowed to equilibrate for 5 minutes before H₂Se gas flow (150 sccm) was turned on. The chamber was held under these conditions for 30 minutes before the tube furnace lid was opened to rapidly cool the chamber. The H₂Se flow was turned off once the temperature decreased below 400°C.

Vibrational Characterization

We performed room temperature Raman spectroscopy using a Horiba LabRam HR Evolution Confocal Microscope with a 100x objective lens (Olympus) and a 633 nm laser filtered to have an intensity of <1 mW. Calibration of the spectra was done using a Si reference sample.

Measurement of Optical Constants

Spectroscopic ellipsometry (SE) on as-grown films was performed with a Woollam RC2 ellipsometer at wavelengths 210-2500 nm and incident angles of 55°, 65°, and 75°. SE of transferred films and bare ALD Al₂O₃/Ag substrates was later performed with a Woollam VASE ellipsometer from 240-900 nm at an incident angle of 65°. The complex permittivity was extracted from the raw Psi-Delta data by fitting the data in the CompleteEASE software (v6.55) with Lorentzian oscillators (See supporting information for details).

Optical Simulation

Absorbance of structures with unpatterned films was calculated using the 1D transfer matrix method. Frequency domain optical simulation of the 1D nanoribbon arrays was done using the Wave Optics module in COMSOL Multiphysics. The system was modeled with monochromatic, normal incidence TM or TE plane waves for incident wavelengths of 400-800 nm in 5 nm increments. The field profiles and power absorption profiles for the 1D nanoribbon arrays were calculated using the finite difference time domain (FDTD) solver in Lumerical. The 2D metasurfaces were similarly modeled using the Lumerical FDTD solver. Both systems were modeled using a normal incidence, broadband plane wave source composed of wavelengths 300 nm to 900 nm and measured at 100 frequency points. The optical constants used for Al₂O₃ were determined using spectroscopic ellipsometry and the constants for Ag are from Palik^[83]. The fraction of light absorbed in the Ag mirror for each structure is determined by integrating the P_{abs} profiles calculated by the Lumerical FDTD solver over the area (for 2D simulations) or volume (3D) of the Ag region. For the 1D nanoribbon arrays, the percent absorption is calculated for TM and TE polarizations. The 2DMSs are both square lattices, so the percent absorption is only calculated for light polarized in the \hat{x} direction.

Metasurface Fabrication

A 1 cm x 1 cm p-Si substrate with a 290 nm thermal oxide was cleaned by sonication in acetone and isopropyl alcohol for 5 minutes each before being blow-dried with N₂. A 100 nm Ag film was deposited by DC sputtering (Kurt J. Lesker P75). The 40 nm thick Al₂O₃ layer was deposited by atomic layer deposition (Cambridge Nanotech) at 150°C at a rate of 0.9Å/cycle for 444 cycles. The precursors for Al and O were trimethyl aluminum (TMA) and H₂O, respectively.

The PtSe₂ films were transferred onto the dielectric/Ag substrates using a wet transfer method. The PtSe₂ films were spin-coated with PMMA A4 (2K rpm, 60s; left to dry overnight) before being removed from the sapphire growth substrate using a ~2 molar potassium hydroxide/water solution. The film was thoroughly cleaned with DI H₂O to remove potassium ions before being transferred to the target substrate. The PMMA was removed by soaking the samples in Remover 1165 on a hot plate set to 80°C for 30 minutes, leaving in room temperature acetone overnight, and then placing the samples in fresh acetone and isopropyl alcohol for 5 minutes each before blow-drying with N₂.

The PtSe₂ films were patterned by electron beam lithography (Elionix ELS-75) and a subsequent dry etch (Oxford RIE 80). ZEP520A E-beam resist diluted with anisole (1:1 by weight) was spin coated at 2K rpm for 60s and baked at 120°C for 3 minutes. Proximity effect correction with a base dose of 225 $\mu\text{C}/\text{cm}^2$ was used for the nanoribbon arrays while the 2D metasurfaces used proximity effect correction with a base dose of 190 $\mu\text{C}/\text{cm}^2$. The samples were then developed using -10°C o-Xylene for 90s before rinsing in room temperature isopropyl alcohol and DI water for 30 seconds each. The film was then etched using reactive ion etching (Oxford RIE 80; 200W RF power, 25 mTorr pressure, 20 sccm CF₄ flow, room temperature) for 28 seconds. Finally, the resist was removed by leaving the samples in Remover 1165 on a hot plate set to 80°C for 2 hours, rinsing with acetone and isopropyl alcohol, and blow-drying with N₂.

Reflectance Measurements

Reflectance measurements were performed at normal incidence with a 50x objective lens (Olympus SLMPLN 50X N.A. = 0.35) in ambient conditions using a confocal microscope (Horiba LabRam HR Evolution) and an external white light source (AvaLight-HAL). The spot size is approximately 4 μm in diameter. For linearly polarized reflectance measurements, a linear polarizer (Edmund Linear Glass Polarizing Filter #43-783) was inserted between the and the sample. Measurements with the linear polarizer were limited to the spectral range of 400 nm to 825 nm due to polarizer bandwidth. Measurements were performed in the dark to minimize noise and the spectra were normalized to a baseline scan taken from the $\text{Al}_2\text{O}_3/\text{Ag}$ coated substrate. A background scan was also collected during which the white light source was turned off. The background was subtracted from each scan:

$$R = \frac{R_{\text{device}} - R_{\text{background}}}{R_{\text{substrate}} - R_{\text{background}}}$$

Scanning Electron Microscope (SEM) Characterization

SEM images of metasurfaces were taken using a FEI Quanta 600 ESEM at an accelerating voltage of 10 kV and with a spot size of 3.0.

Acknowledgements

D.J., A.A. and J.L. acknowledge primary support for this work by the Asian Office of Aerospace Research and Development (AOARD) of the Air Force Office of Scientific Research (AFOSR) FA2386-20-1-4074 and FA2386-21-1-4063. D.J. also acknowledges partial support from the University Research Foundation at Penn and the Alfred P. Sloan Foundation for the Sloan Fellowship. D.J., P.K. and H. Z. acknowledge support from the National Science Foundation (NSF) (grant no. DMR-1905853) and support from University of Pennsylvania Materials Research Science and Engineering Center (MRSEC) (grant no. DMR-1720530) in addition to usage of MRSEC supported facilities. The sample fabrication, assembly and characterization were carried out at the Singh Center for Nanotechnology at the University of Pennsylvania, which is supported by the NSF National Nanotechnology Coordinated Infrastructure Program grant no. NNCI-1542153. F.B. is supported by the Vagelos Integrated Program in Energy Research. H.Z. was partially supported by Vagelos Institute of Energy Science and Technology graduate fellowship. J.R.H. acknowledges support from the Air Force Office of Scientific Research (Program Manager Dr. Gernot Pomrenke) under award number FA9550-20RYCOR059. M. S. and N. R. G. acknowledge support from the Air Force Office of Scientific Research under Award No. FA9550-19RYCOR050. Dr. Evan Smith helped with preliminary ellipsometry measurements.

References

- [1] J. B. Pendry, D. Schurig, D. R. Smith, *Science* (80-.). **2006**, *312*, 1780.
- [2] A. V. Kildishev, A. Boltasseva, V. M. Shalaev, *Science* (80-.). **2013**, *339*, 1232009.
- [3] C. M. Watts, X. Liu, W. J. Padilla, *Adv. Mater.* **2012**, *24*, 98.
- [4] Z. Li, S. Butun, K. Aydin, *ACS Photonics* **2015**, *2*, 183.
- [5] N. Liu, M. Mesch, T. Weiss, M. Hentschel, H. Giessen, *Nano Lett.* **2010**, *10*, 2342.
- [6] P. Yu, L. V. Besteiro, Y. Huang, J. Wu, L. Fu, H. H. Tan, C. Jagadish, G. P. Wiederrecht, A. O. Govorov, Z.

- Wang, *Adv. Opt. Mater.* **2019**, *7*, 1.
- [7] Z. Yuan, P. C. Wu, Y. C. Chen, *Laser Photonics Rev.* **2022**, *16*, 1.
- [8] Y.-L. Liao, J. Zhou, X. Chen, J. Wu, Z. Chen, S. Wu, Y. Zhao, *Opt. Express* **2022**, *30*, 16847.
- [9] T. P. Pasanen, J. Isometsä, M. Garin, K. Chen, V. Vähänissi, H. Savin, *Adv. Opt. Mater.* **2020**, *8*, 2000047.
- [10] E. Garnett, P. Yang, *Nano Lett.* **2010**, *10*, 1082.
- [11] M. M. Hassan, F. Islam, M. Z. Baten, S. Subrina, *RSC Adv.* **2021**, *11*, 37595.
- [12] K. Mizuno, J. Ishii, H. Kishida, Y. Hayamizu, S. Yasuda, D. N. Futaba, M. Yumura, K. Hata, *Proc. Natl. Acad. Sci. U. S. A.* **2009**, *106*, 6044.
- [13] K. T. Fountaine, W. H. Cheng, C. R. Bukowsky, H. A. Atwater, *ACS Photonics* **2016**, *3*, 1826.
- [14] J. Zhu, Z. Yu, G. F. Burkhardt, C. M. Hsu, S. T. Connor, Y. Xu, Q. Wang, M. McGehee, S. Fan, Y. Cui, *Nano Lett.* **2009**, *9*, 279.
- [15] F. Ding, Y. Jin, B. Li, H. Cheng, L. Mo, S. He, *Laser Photonics Rev.* **2014**, *8*, 946.
- [16] K. Aydin, V. E. Ferry, R. M. Briggs, H. A. Atwater, *Nat. Commun.* **2011**, *2*, 1.
- [17] K. Chaudhuri, M. Alhabeab, Z. Wang, V. M. ShalaeV, Y. Gogotsi, A. Boltasseva, *ACS Photonics* **2018**, *5*, 1115.
- [18] S. A. Maier, M. L. Brongersma, P. G. Kik, S. Meltzer, A. A. G. Requicha, H. A. Atwater, *Adv. Mater.* **2001**, *13*, 1501.
- [19] F. Ding, Y. Yang, R. A. Deshpande, S. I. Bozhevolnyi, *Nanophotonics* **2018**, *7*, 1129.
- [20] W. L. Barnes, A. Dereux, T. W. Ebbesen, *Nature* **2003**, *424*, 824.
- [21] J.-J. Chen, J. C. S. Wu, P. C. Wu, D. P. Tsai, *J. Phys. Chem. C* **2011**, *115*, 210.
- [22] P. Berini, *Laser Photonics Rev* **2013**, *8*, 197.
- [23] W. Li, J. Valentine, *Nano Lett.* **2014**, *14*, 3510.
- [24] Y. H. Jang, Y. J. Jang, S. Kim, L. N. Quan, K. Chung, D. H. Kim, *Chem. Rev.* **2016**, *116*, 14982.
- [25] Y. Cui, Y. He, Y. Jin, F. Ding, L. Yang, Y. Ye, S. Zhong, Y. Lin, S. He, *Laser Photonics Rev.* **2014**, *8*, 495.
- [26] T. V. Teperik, F. J. García De Abajo, A. G. Borisov, M. Abdelsalam, P. N. Bartlett, Y. Sugawara, J. J. Baumberg, *Nat. Photonics* **2008**, *2*, 299.
- [27] W. C. Wang, P. Garu, *Sci. Rep.* **2022**, *12*, 1.
- [28] Y. Cui, J. Xu, K. Hung Fung, Y. Jin, A. Kumar, S. He, N. X. Fang, *Appl. Phys. Lett.* **2011**, *99*, 253101.
- [29] J. Hendrickson, J. Guo, B. Zhang, W. Buchwald, R. Soref, *Opt. Lett.* **2012**, *37*, 371.
- [30] J. R. Hendrickson, S. Vangala, C. Dass, R. Gibson, J. Goldsmith, K. Leedy, D. E. Walker, J. W. Cleary, W. Kim, J. Guo, *ACS Photonics* **2018**, *5*, 776.
- [31] F. Ding, J. Dai, Y. Chen, J. Zhu, Y. Jin, S. I. Bozhevolnyi, *Sci. Rep.* **2016**, *6*, 1.
- [32] M. Xu, L. Guo, P. Zhang, Y. Qiu, Q. Li, J. Wang, *RSC Adv.* **2022**, *12*, 16823.
- [33] R. M. H. Bilal, M. A. Saeed, P. K. Choudhury, M. A. Baqir, W. Kamal, M. M. Ali, A. A. Rahim, *Sci. Rep.* **2020**, *10*, 1.
- [34] M. Chirumamilla, A. S. Roberts, F. Ding, D. Wang, P. K. Kristensen, S. I. Bozhevolnyi, K. Pedersen, *Opt. Mater. Express* **2016**, *6*, 2704.
- [35] A. S. Rana, M. Q. Mehmood, H. Jeong, I. Kim, J. Rho, *Sci. Rep.* **2018**, *8*, 2.
- [36] S. Wang, F. Chen, R. Ji, M. Hou, F. Yi, W. Zheng, T. Zhang, W. Lu, *Adv. Opt. Mater.* **2019**, *7*, 1.
- [37] Q. Qian, T. Sun, Y. Yan, C. Wang, *Adv. Opt. Mater.* **2017**, *5*, 1.
- [38] W. Li, U. Guler, N. Kinsey, G. V. Naik, A. Boltasseva, J. Guan, V. M. ShalaeV, A. V. Kildishev, *Adv. Mater.* **2014**, *26*, 7959.
- [39] D. Jariwala, A. R. Davoyan, G. Tagliabue, M. C. Sherrott, J. Wong, H. A. Atwater, *Nano Lett* **2016**, *16*, 8.
- [40] P. Kumar, J. Lynch, B. Song, H. Ling, F. Barrera, K. Kisslinger, H. Zhang, S. B. Anantharaman, J. Digani, H. Zhu, T. H. Choudhury, C. McAleese, X. Wang, B. R. Conran, O. Whear, M. J. Motala, M. Snure, C. Muratore, J. M. Redwing, N. R. Glavin, E. A. Stach, A. R. Davoyan, D. Jariwala, *Nat. Nanotechnol.* **2022**, *17*, 182.
- [41] H. Zhang, B. Abhiraman, Q. Zhang, J. Miao, K. Jo, S. Roccacesecca, M. W. Knight, A. R. Davoyan, D. Jariwala, *Nat. Commun.* **2020**, *11*, 3552.
- [42] B. Cao, Z. Ye, L. Yang, L. Gou, Z. Wang, *Nanotechnology* **2021**, *32*, DOI: 10.1088/1361-6528/ac0d7c.
- [43] X. Chia, Z. Sofer, J. Luxa, M. Pumera, *ACS Appl. Mater. Interfaces* **2017**, *9*, 25587.
- [44] X. Chia, A. Adriano, P. Lazar, Z. Sofer, J. Luxa, M. Pumera, *Adv. Funct. Mater.* **2016**, *26*, 4306.
- [45] D. Kireev, E. Okogbue, R. T. Jayanth, T. J. Ko, Y. Jung, D. Akinwande, *ACS Nano* **2021**, *15*, 2800.
- [46] X. Chen, J. Huang, C. Chen, M. Chen, G. Hu, H. Wang, N. Dong, J. Wang, *Adv. Opt. Mater.* **2022**, *10*, 1.
- [47] Y. Zhao, J. Qiao, Z. Yu, P. Yu, K. Xu, S. P. Lau, W. Zhou, Z. Liu, X. Wang, W. Ji, Y. Chai, *Adv. Mater.* **2017**, *29*, DOI: 10.1002/adma.201604230.

- [48] H. J. Noh, J. Jeong, E. J. Cho, K. Kim, B. I. Min, B. G. Park, *Phys. Rev. Lett.* **2017**, *119*, 1.
- [49] Y. Wang, L. Li, W. Yao, S. Song, J. T. Sun, J. Pan, X. Ren, C. Li, E. Okunishi, Y. Q. Wang, E. Wang, Y. Shao, Y. Y. Zhang, H. T. Yang, E. F. Schwier, H. Iwasawa, K. Shimada, M. Taniguchi, Z. Cheng, S. Zhou, S. Du, S. J. Pennycook, S. T. Pantelides, H. J. Gao, *Nano Lett.* **2015**, *15*, 4013.
- [50] R. Angelo, B. Villaos, C. P. Crisostomo, Z.-Q. Huang, S.-M. Huang, A. Abraham, B. Padama, M. A. Albao, H. Lin, F.-C. Chuang, *npj 2D Mater. Appl.* **2019**, *3*, DOI: 10.1038/s41699-018-0085-z.
- [51] H. Huang, S. Zhou, W. Duan, *Phys. Rev. B* **2016**, *94*, 1.
- [52] K. Zhang, M. Yan, H. Zhang, H. Huang, M. Arita, Z. Sun, W. Duan, Y. Wu, S. Zhou, *Phys. Rev. B* **2017**, *96*, 125102.
- [53] J. He, W. Jiang, X. Zhu, R. Zhang, J. Wang, M. Zhu, S. Wang, Y. Zheng, L. Chen, *Phys. Chem. Chem. Phys.* **2020**, *22*, 26383.
- [54] G. A. Ermolaev, K. V. Voronin, M. K. Tatmyshevskiy, A. B. Mazitov, A. S. Slavich, D. I. Yakubovskiy, A. P. Tselin, M. S. Mironov, R. I. Romanov, A. M. Markeev, I. A. Kruglov, S. M. Novikov, A. A. Vyshnevyy, A. V. Arsenin, V. S. Volkov, *Nanomaterials* **2021**, *11*, 1.
- [55] J. Yuan, H. Mu, L. Li, Y. Chen, W. Yu, K. Zhang, B. Sun, S. Lin, S. Li, Q. Bao, *ACS Appl. Mater. Interfaces* **2018**, *10*, 21534.
- [56] C. Yim, K. Lee, N. McEvoy, M. O'Brien, S. Riazimehr, N. C. Berner, C. P. Cullen, J. Kotakoski, J. C. Meyer, M. C. Lemme, G. S. Duesberg, *ACS Nano* **2016**, *10*, 9550.
- [57] F. Bonell, A. Marty, C. Vergnaud, V. Consonni, H. Okuno, A. Ouerghi, H. Boukari, M. Jamet, *2D Mater.* **2022**, *9*, DOI: 10.1088/2053-1583/ac37aa.
- [58] X. Yong, J. Zhang, X. Ma, *Int. J. Hydrogen Energy* **2020**, *45*, 8549.
- [59] X. Meng, Y. Shen, J. Liu, L. Lv, X. Yang, X. Gao, M. Zhou, X. Wang, Y. Zheng, Z. Zhou, *Appl. Catal. A Gen.* **2021**, *624*, 118332.
- [60] D. Hu, T. Zhao, X. Ping, H. Zheng, L. Xing, X. Liu, J. Zheng, L. Sun, L. Gu, C. Tao, D. Wang, L. Jiao, *Angew. Chemie* **2019**, *131*, 7051.
- [61] S. Lin, Y. Liu, Z. Hu, W. Lu, C. H. Mak, L. Zeng, J. Zhao, Y. Li, F. Yan, Y. H. Tsang, X. Zhang, S. P. Lau, *Nano Energy* **2017**, *42*, 26.
- [62] X. Sun, H. Zhang, X. Li, Y. Z. Zheng, J. Wu, N. Li, H. Ding, X. Lv, X. Tao, *Energy Technol.* **2020**, *8*, 1.
- [63] Y. Chang, P. Zhai, J. Hou, J. Zhao, J. Gao, *Adv. Energy Mater.* **2022**, *12*, 1.
- [64] S. Lukas, O. Hartwig, M. Prechtel, G. Capraro, J. Boltzen, A. Meledin, J. Mayer, D. Neumaier, S. Kataria, G. S. Duesberg, M. C. Lemme, *Adv. Funct. Mater.* **2021**, *31*, 2102929.
- [65] M. O'Brien, N. McEvoy, C. Motta, J. Y. Zheng, N. C. Berner, J. Kotakoski, K. Elibol, T. J. Pennycook, J. C. Meyer, C. Yim, M. Abid, T. Hallam, J. F. Donegan, S. Sanvito, G. S. Duesberg, *2D Mater.* **2016**, *3*, DOI: 10.1088/2053-1583/3/2/021004.
- [66] S. Parhizkar, M. Prechtel, A. L. Giesecke, S. Suckow, S. Wahl, S. Lukas, O. Hartwig, N. Negm, A. Quellmalz, K. Gylfason, D. Schall, M. Wuttig, G. S. Duesberg, M. C. Lemme, *ACS Photonics* **2022**, *9*, 859.
- [67] F. Ghasemi, R. Taghavimendi, A. Bakhshayeshi, *Opt. Quantum Electron.* **2020**, *52*, 492.
- [68] X. Li, D. Han, F. Wu, C. Xu, X. Liu, J. Zi, *J. Phys. Condens. Matter* **2008**, *20*, DOI: 10.1088/0953-8984/20/48/485001.
- [69] T. R. Cook, D. K. Dogutan, S. Y. Reece, Y. Surendranath, T. S. Teets, D. G. Nocera, *Chem. Rev.* **2010**, *110*, 6474.
- [70] L. Wang, L. Han, W. Guo, L. Zhang, C. Yao, Z. Chen, Y. Chen, C. Guo, K. Zhang, C.-N. Kuo, C. Shan Lue, A. Politano, H. Xing, M. Jiang, X. Yu, X. Chen, W. Lu, *Light Sci. Appl.* **2022**, *11*, 53.
- [71] D. E. Aspnes, A. A. Studna, *Phys. Rev. B* **1983**, *27*, 985.
- [72] S. Mehrabi, R. M. H. Bilal, M. A. Naveed, M. M. Ali, *Opt. Mater. Express* **2022**, *12*, 2199.
- [73] C. Ng, L. W. Yap, A. Roberts, W. Cheng, D. E. Gómez, *Adv. Funct. Mater.* **2017**, *27*, DOI: 10.1002/adfm.201604080.
- [74] R. A. Pala, S. Butun, K. Aydin, H. A. Atwater, *Sci. Rep.* **2016**, *6*, 1.
- [75] J. Park, J. H. Kang, A. P. Vasudev, D. T. Schoen, H. Kim, E. Hasman, M. L. Brongersma, *ACS Photonics* **2014**, *1*, 812.
- [76] Q. Shi, T. U. Connell, Q. Xiao, A. S. R. Chesman, W. Cheng, A. Roberts, T. J. Davis, D. E. Gómez, *ACS Photonics* **2019**, *6*, 314.
- [77] M. C. Soydan, A. Ghodabi, D. U. Yildirim, V. B. Erturk, E. Ozbay, *Plasmonics* **2019**, *14*, 1801.
- [78] F. Tan, N. Wang, D. Y. Lei, W. Yu, X. Zhang, *Adv. Opt. Mater.* **2017**, *5*, DOI: 10.1002/adom.201600399.
- [79] H. Zhang, K. Wu, *J. Opt. Soc. Am. B* **2022**, *39*, 332.
- [80] W. Dong, Y. Qiu, J. Yang, R. E. Simpson, T. Cao, *J. Phys. Chem. C* **2016**, *120*, 12713.

- [81] Q. Xiao, C. Kinnear, T. U. Connell, M. K. Kashif, C. D. Easton, A. Seeber, L. Bourgeois, G. O. Bonin, N. W. Duffy, A. S. R. Chesman, D. E. Gómez, *ACS Appl. Nano Mater.* **2021**, *4*, 2702.
- [82] E. U. Biswas, S. M. Sahel, M. M. E. Kamal, S. Mahmud, S. Biswas, S. S. Hassan, M. R. C. Mahdy, *Opt. Mater. Express* **2022**, *12*, 2102.
- [83] E. D. Palik, *Handbook of Optical Constants of Solids*, Elsevier Inc., **1985**.

Supporting Information: Ultrathin Broadband Metasurface Superabsorber Based on a van der Waals Semimetal

Adam D. Alfieri¹, Michael J. Motala², Michael Snure³, Jason Lynch¹, Pawan Kumar^{1,4}, Huiqin Zhang¹, Susanna Post⁵, Christopher Muratore⁵, Joshua R. Hendrickson³, Nicholas R. Glavin^{*6}, Deep Jariwala^{*1}.

¹Department of Electrical and Systems Engineering, University of Pennsylvania, Philadelphia, PA 19104, USA

²UES Inc. Dayton, OH, 45432

³Air Force Research Laboratory, Sensors Directorate, Wright-Patterson Air Force Base, OH, 45433, USA

⁴Department of Materials Science and Engineering, University of Pennsylvania, Philadelphia, PA 19104, USA

⁵Department of Chemical and Materials Engineering, University of Dayton, Dayton, OH, 45469, USA

⁶Air Force Research Laboratory, Materials and Manufacturing Directorate, Wright-Patterson Air Force Base, OH, 45433, USA

*Corresponding Authors: dmj@seas.upenn.edu; nicholas.glavin.1@afrl.af.mil

S1. Growth and Characterization

S1.1. Growth and Structural Characterization

In the initial optimization of the growth conditions, we annealed Pt in H₂Se at temperatures ranging from 375°C to 650°C. Temperature dependent Raman and XRD data are shown in Figure S1, showing the synthesis of PtSe₂ at temperatures ranging from 375°C to 650°C. The presence of the E_g and A_{1g} Raman peaks at 178 cm⁻¹ and 206 cm⁻¹ for all growth conditions shows the formation of crystalline PtSe₂ at all 3 temperatures. The presence of the PtSe₂ peaks and lack of any Pt peaks in the XRD confirm the complete selenization of the Pt film.

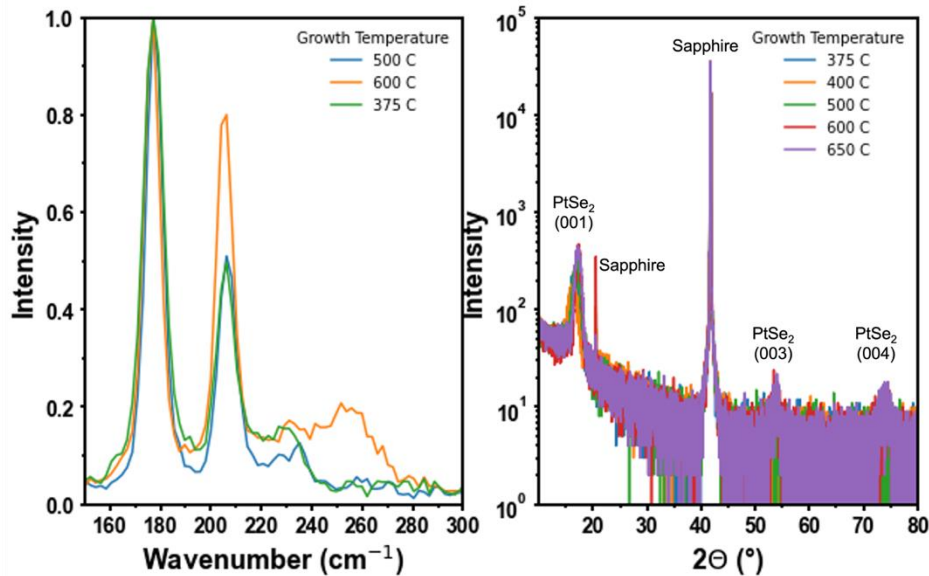


Figure S1. Raman spectra (a) and x-ray diffraction scans (b) for different growth temperatures.

Cross-sectional transmission electron microscopy (X-TEM) was performed on a PtSe₂ film transferred to a SiO₂/Si substrate (Figure S2). The X-TEM sample was fabricated with a dual beam plasma-focus ion beam (FIB) setup. A soft carbon layer (using Sharpie marker) was coated on top of the PtSe₂ film to avoid the contamination as well as beam damages while preparing the

specimen. 30 keV to 5 keV ion beam were used for the specimen preparation for milling, thinning, and polishing along with an in-situ liftoff processes. The as prepared X-TEM specimen attached to the Omniprobe half grid was analyzed under high angle annular dark field (HAADF) scanning transmission electron microscopy (STEM). Aberration corrected (probe correction) STEM uses a probe size of $\sim 1\text{\AA}$ and accelerating voltage of 200kV. A high speed large dual detector was used to get ultra-high resolution EDS mapped images. The van der Waals layered structure of PtSe₂ can be easily seen, and the vdW layers are horizontally aligned. The domain size of this nanocrystalline PtSe₂ ranges from 50 to 100 nm. Moreover, the HAADF STEM image and elemental mapping confirm complete selenization of the platinum to form PtSe₂ layers.

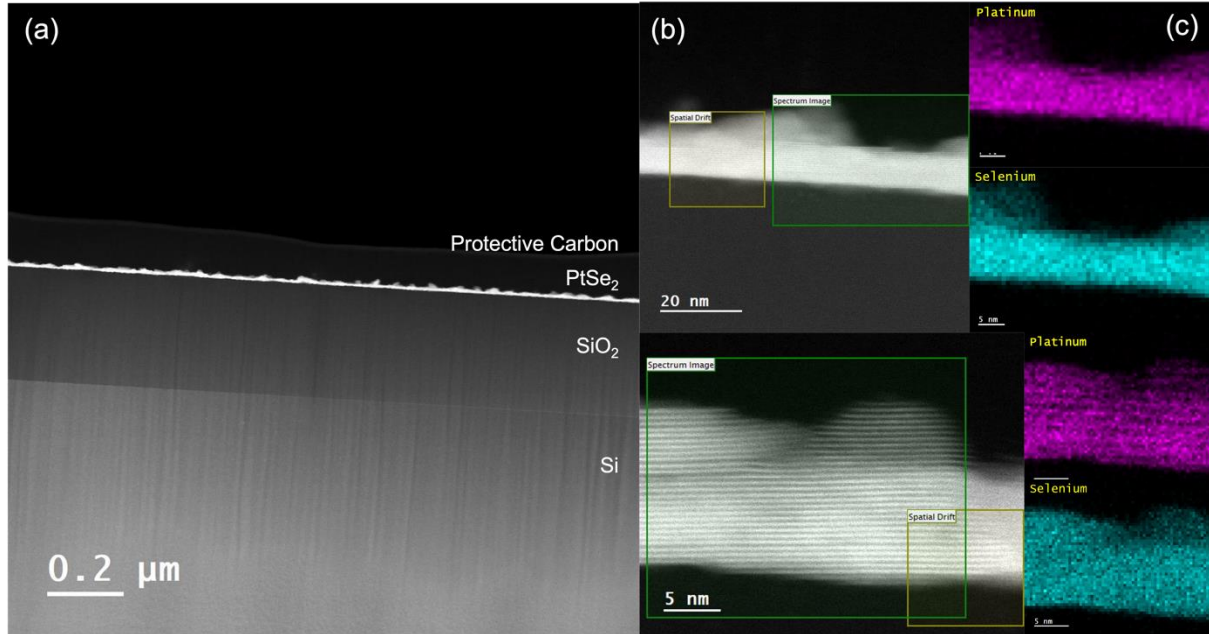


Figure S2. Cross-Sectional Scanning Transmission Electron Microscope (X-STEM) Analysis. (a) Low magnification cross sectional high angle annular dark field (HAADF) scanning transmission electron micrograph image of a PtSe₂ film transferred onto SiO₂/Si and coated with a protective carbon layer. (b) High magnification HAADF X-STEM images of the sample at two different spots and (c) the corresponding elemental mapping. The green boxes in (b) are the range over which the elemental mapping is performed.

S1.2. Ellipsometry and Optical Constants

S1.2.1. Measurement and Fitting

Spectroscopic ellipsometry (SE) measures the ratio of complex reflection coefficients for *s* and *p* polarized light:

$$\frac{r_p}{r_s} = \tan(\psi)e^{-i\Delta} \quad (1)$$

The measured ψ and Δ values (Figure S3) are related to the dielectric function of the medium. The dielectric function and complex refractive index are determined by fitting the raw ψ and Δ . We fit

the ψ and Δ values with a background term, ϵ_∞ , a UV pole, an IR pole, and a series of four Lorentz oscillators:

$$\epsilon(E) = \epsilon_\infty + \frac{A_{UV}}{E_{UV}^2 - E^2} - \frac{A_{IR}}{E^2} + \sum_j \frac{A_j \Gamma_j E_j}{E_j^2 - E^2 - i\Gamma_j E_j} \quad (2)$$

The model parameters are given in Table 1, and the fits are plotted against the raw data in Figure S3 to confirm the validity of the model.

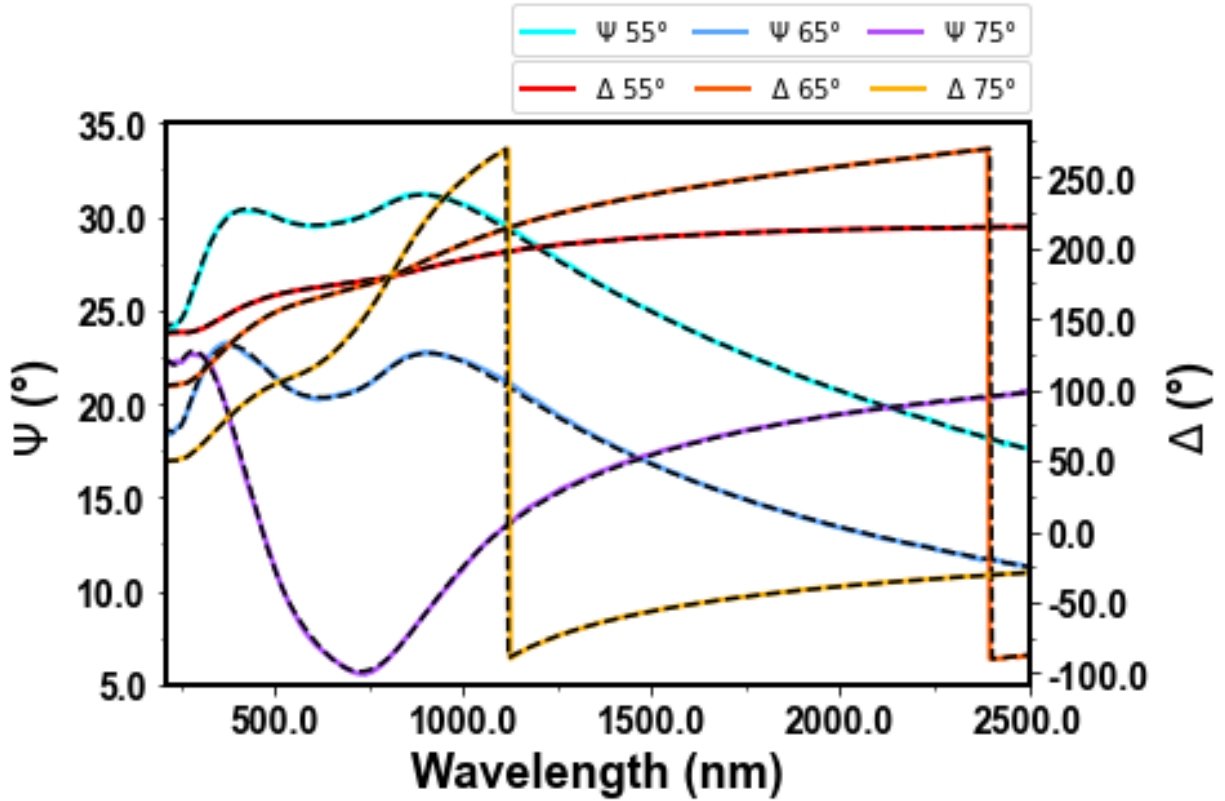


Figure S3. Experimental Psi-Delta values for the as-grown films on sapphire measured by SE. Measured data taken at incident angles of 55-75° in 10° increments is shown, and the corresponding fits from the model are overlaid (black dashed lines).

Figure S4 shows the optical constants of as-grown films annealed at different temperatures. We see that the optical properties of the films are highly dependent on the growth temperature. Growth at 500-550°C appears to be necessary to achieve a plasmonic response, as this zero-crossing of ϵ' becomes negligible for films grown at higher and lower temperatures. Moreover, the interband absorption is maximized in this temperature range.

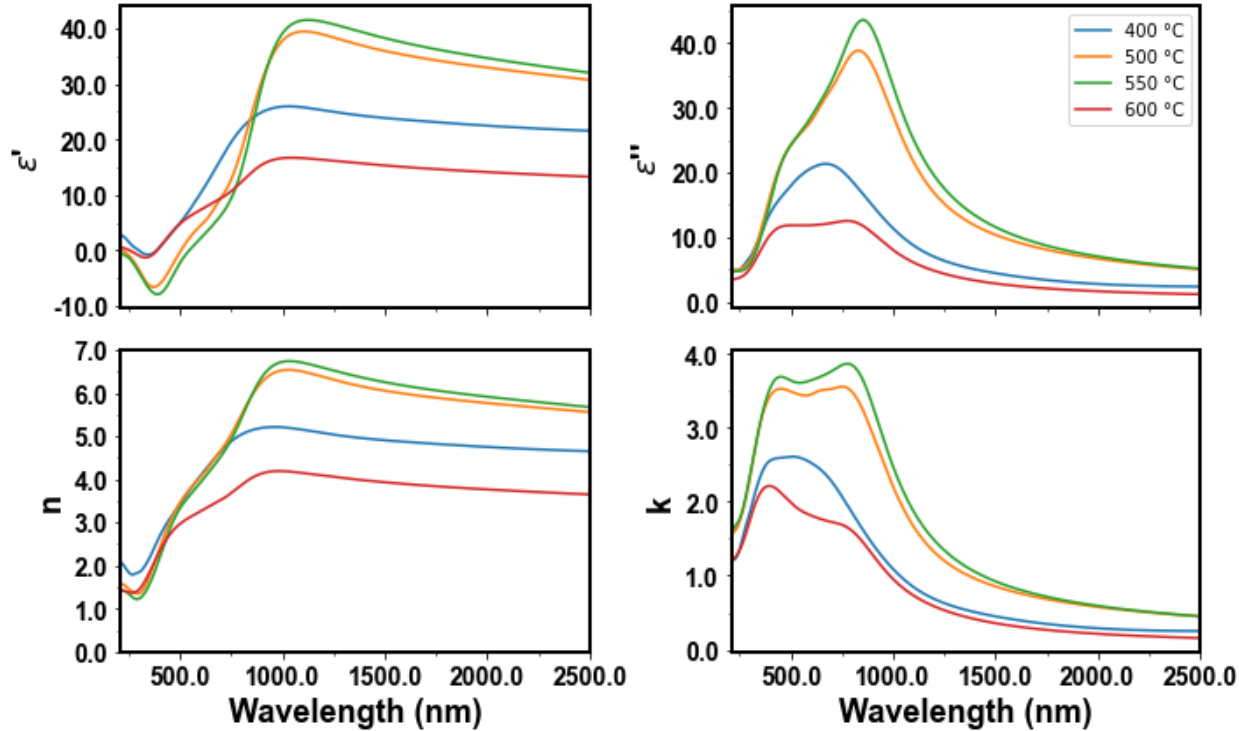


Figure S4. Optical constants of as-grown PtSe₂ as a function of growth temperature for growth temperatures ranging from 400°C to 600°C. We see that the best optical properties are achieved at growth temperatures of 500-550°C.

S1.2.2. Transfer-Induced Change in Optical Properties and Thickness

We observed a change in the thickness and optical properties of the PtSe₂ after transfer. We expect that this is the result of the nanocrystalline structure “breaking apart” at the grain boundaries, leading to a decreased density. The optical properties of the transferred film (Figures 1c of main MS) differ from those of the as grown film (Figure S4): the magnitude of the constants decreases after transfer. The measured ψ - Δ data from SE of the transferred film was fit with 4 Lorentzian oscillators (Table 1). The raw data (solid lines) and the fit (dashed lines) are plotted in Figure S5. The discrepancies can likely be explained by the roughness of the underlying substrate, wrinkles of the transferred film, and the roughness of the film itself. The fit is reasonably good for the wavelengths of interest (400 nm to 900 nm).

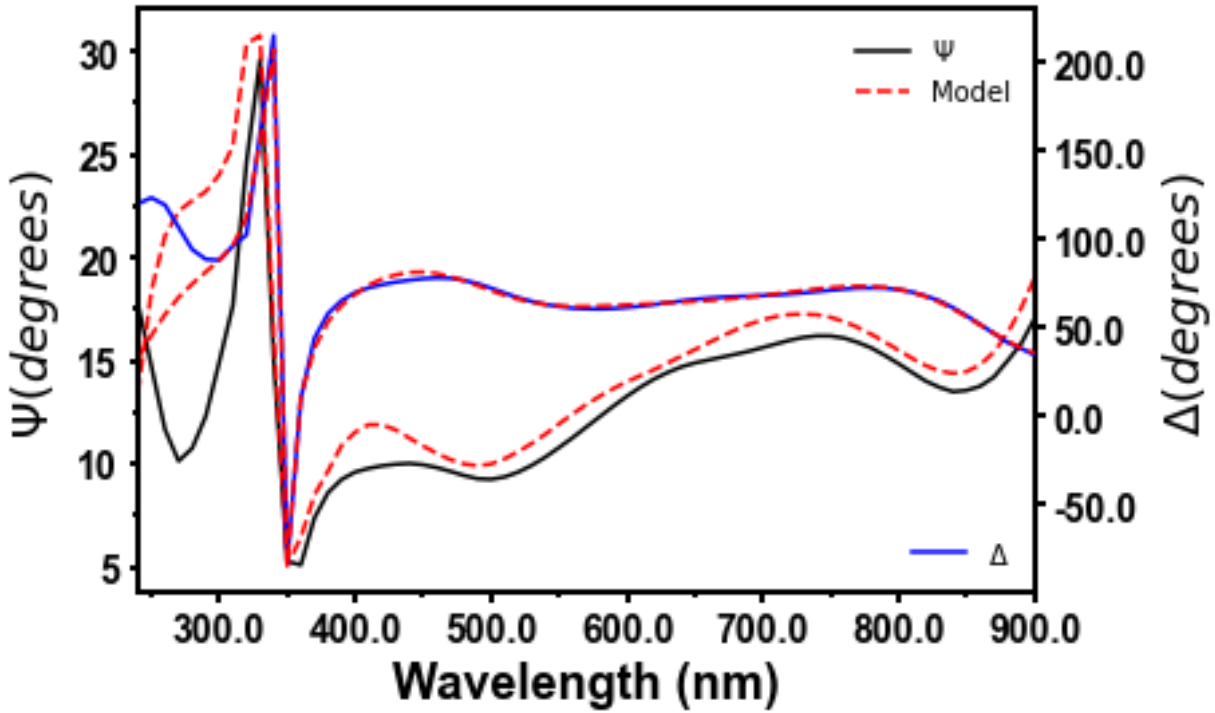


Figure S5, Experimental Psi-Delta from ellipsometry taken at an incident angle of 65° and the corresponding fits from the model (red dashed lines).

S2. Nanoribbon Device Characterization

S2.1. Device Images

In Figures S6a and S6b, we show scanning electron micrographs of devices with a nominal w of 50 nm ($p = 150$ nm) and $w = 80$ nm ($p = 240$ nm), respectively. We show measurements on the SEM images to confirm the dimensions. In Figure S6c, we show an atomic force micrograph of a device with a nominal w of 90 nm ($p = 270$ nm). While the AFM tip cannot fully resolve the lateral dimensions, we see that the PtSe₂ is indeed being removed fully by the etching process.

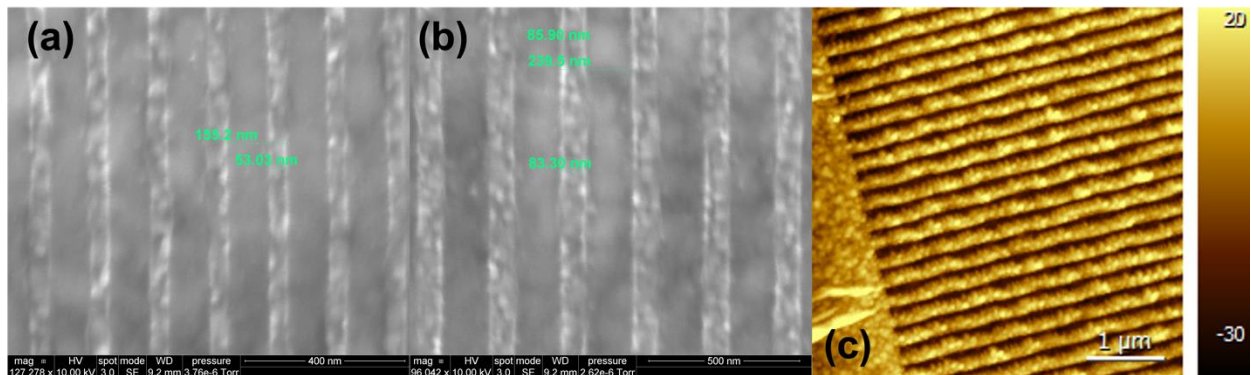


Figure S6. SEM and AFM Images of nanoribbon devices.

S2.2. Characterization of Nanoribbon Array Modes

S2.2.1. Field Profiles of Modes P1 and P2

Illumination by TM light excites two plasmon modes, the $|E|$, $\text{Re}(E_x)$, and $\text{Re}(E_y)$ field profiles are shown in figure S7. A lower energy plasmon mode (P1, top) is localized above and below the nanoribbon. The higher energy mode (P2, bottom) is localized to the sides of the nanoribbon. Both modes can be considered gap surface plasmon (GSP) like modes. Metal-insulator-metal (MIM) structures for GSP modes can be thought of as Fabry-Perot (FP) cavities with a large mode index^[1]. This, of course, requires sufficient reflectance at each interface for multiple reflections to occur. The impedance mismatch between the PtSe₂ and alumina layer results in reflectance values of ~ 0.25 at 640 nm and ~ 0.3 at 425 nm for light travelling from the alumina incident on the PtSe₂. The structure consequently behaves like a lossy FP cavity and supports GSP-like modes.

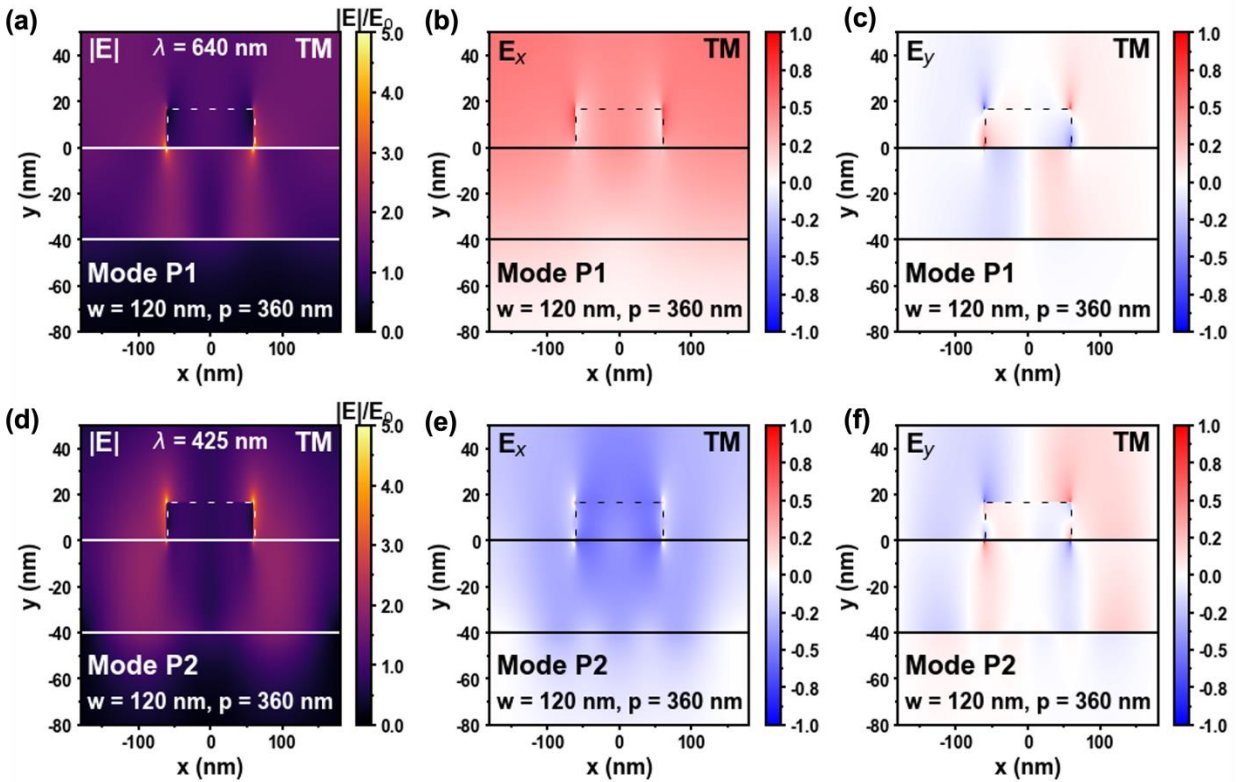


Figure S7. TM Modes of PtSe₂ Nanoribbon Devices. (a) $|E|$ field profiles, (b) $\text{Re}(E_x)$ field profiles, and (c) $\text{Re}(E_y)$ for the P1 ($\lambda = 640$ nm, top) and P2 ($\lambda = 425$ nm, bottom) modes for a nanoribbon array with $w = 120$ nm and $p = 360$ nm. The $\text{Re}(E_x)$ and $\text{Re}(E_y)$ profiles are normalized to themselves.

S2.2.2. Origin of Plasmon Resonances

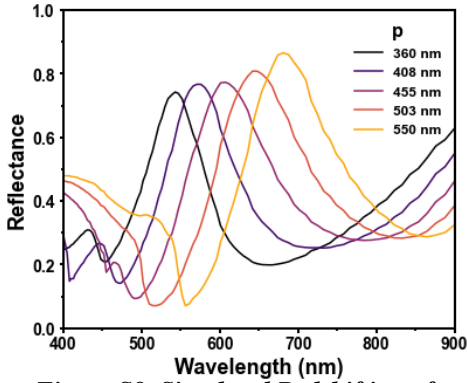


Figure S8. Simulated Redshifting of P2 Mode Beyond 470 nm. Simulated reflectance spectra of the PtSe₂ nanoribbon structure (17 nm PtSe₂/40 nm Al₂O₃/100 nm Ag) illuminated by TM polarized plane wave. In the simulation, the period p is varied while the fill factor is fixed at 1/3.

To better understand the role of the PtSe₂ and Ag, we performed a control simulation for which we replaced the PtSe₂ nanoribbons with a fictitious (and non-physical) material that has the same n as PtSe₂ but has $k = 0$. Figure S9a shows the calculated TM absorbance spectra for a control device with $w = 120$ nm, $p = 360$ nm. There is a strong absorbance peak at 550 nm due to the P1 mode (Figure S9b) and a small peak at approximately 415 nm due to the P2 mode (Figure S9c). The locations and field profiles of these two modes are in good agreement with the P1 and P2 modes shown in Figure 3 of the main manuscript. We also note that off resonance absorption is minimal, further supporting our main argument that absorbance is due to interband loss in PtSe₂, with Ag assisting. Further, while PtSe₂ is optically a metal ($\text{Re}(\epsilon) < 0$) below 470 nm, it can also be shown by simulation that the P2 mode can be shifted to wavelengths where PtSe₂ is optically a dielectric (Figure S8). We can

therefore attribute both modes to the silver.

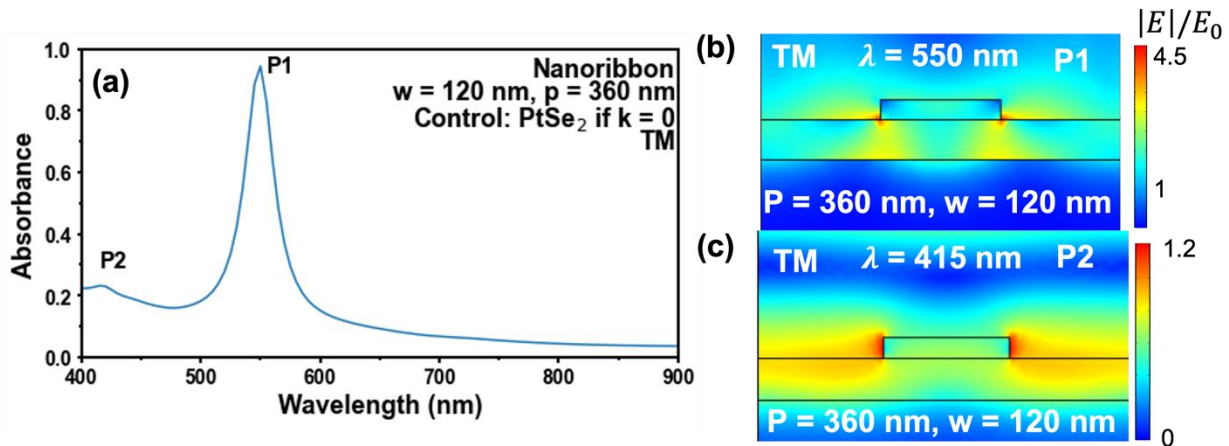


Figure S9. Control Simulations of Nanoribbons with $n = n(\text{PtSe}_2)$ and $k = 0$. (a) Simulated absorbance spectrum of a control device with $w = 120$ nm, $p = 360$ nm, and the material $k = 0$ under illumination by a TM polarized plane wave. The P1 and P2 modes are labeled in the spectrum, and the $|E|$ field profiles the P1 and P2 modes are shown in (b) and (c), respectively.

S2.2.3. Waveguide Mode

For TM polarized light, in experimental spectra, we see the emergence of a third peak (labeled ‘WG’ in Figure 2c) that is not predicted by normal incidence simulations. We find that this is a waveguide-like resonance that emerges at non-zero angles of incidence at ~ 2.35 eV for a device with $w = 120$ nm and $p = 3w$ (Figure S10). Experimentally, this is the result of the numerical aperture of the microscope being ~ 0.35 , resulting in incident angles up to approximately 20.5° .

S2.2.4. Effect of Dielectric Layer Permittivity

Plasmons are dependent on the local dielectric environment^[2]. For our system, we expect the effective dielectric permittivity of the surrounding environment to be approximately proportional to $(1 + \epsilon_s)$, where ϵ_s is the relative permittivity of the dielectric spacer layer. We then expect the plasmon frequency, ω_p , to vary as:

$$\omega_p \propto (1 + \epsilon_s)^{-1/2} \quad (3)$$

Figure S11a shows the reflectance magnitude as a function of energy and ϵ_s for a device with $w = 90$ nm, $p = 270$ nm, and $t = 40$ nm. We observe that both the P1 and P2 modes follow the expected dispersion given by (3).

S2.2.5. Effect of Dielectric Layer Thickness

As mentioned in S2.2.1., the structure has a GSP-like response that consequently depends on the thickness of the dielectric layer. We would expect a ‘‘pure’’ GSP resonance to redshift with increasing layer thickness t . In Figure S11b, we plot the simulated reflectance magnitude as a function of t and energy for a device with an Al_2O_3 dielectric, $w = 120$ nm, and $p = 360$ nm. Two phenomena are observed: (i.) modes redshift with increasing t and (ii.) changing t causes different modes to have enhanced absorption for devices with the same width and period. Thinner layers have a higher cavity photon energy and therefore couple to the higher energy P2 mode while thicker layers couple to the P1 mode. The dielectric thickness should be chosen to optimize both plasmon energy and reflectance magnitude.

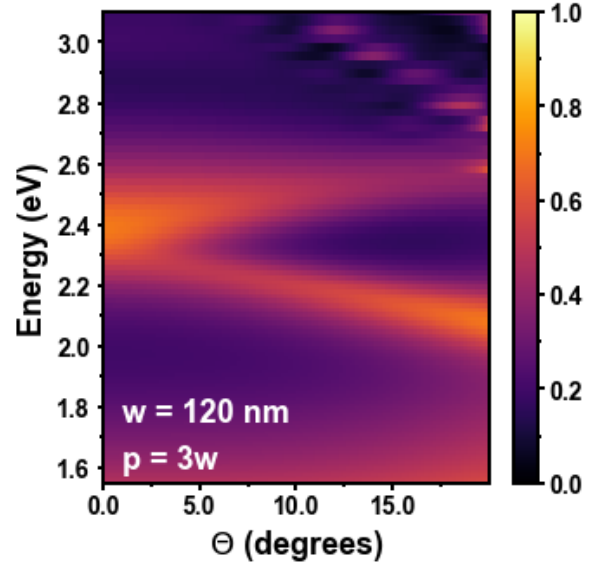


Figure S10. Waveguide mode. Simulated reflectance of a device on 40 nm Al_2O_3 with $w = 120$ nm and $p = 360$ nm as a function of incident angle and energy. At angles greater than $\approx 5^\circ$, the reflectance maximum splits into two peaks, and a reflectance minimum arises.

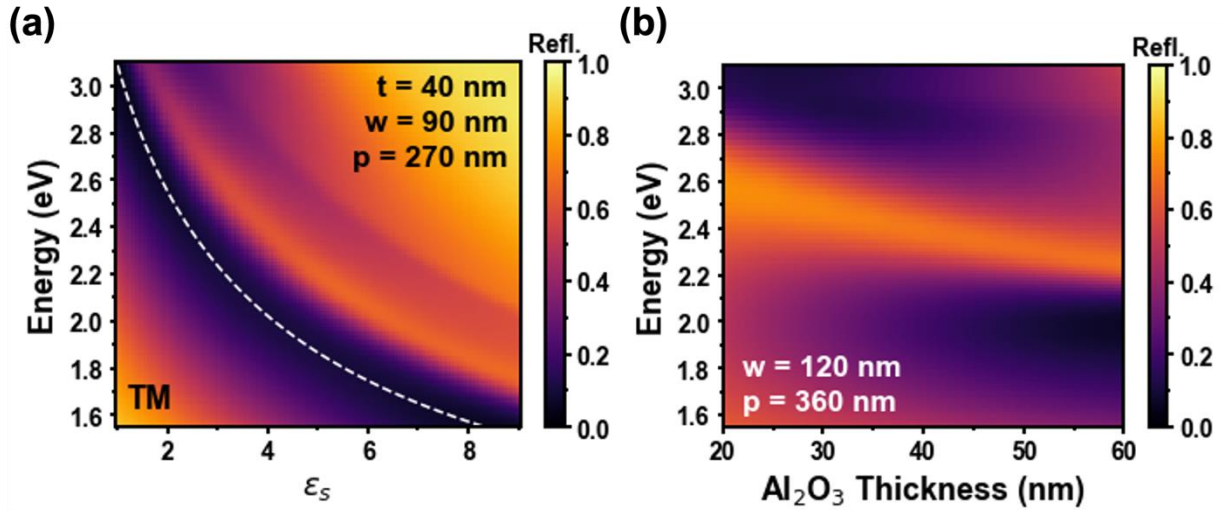


Figure S11. Effects of (a) Dielectric Permittivity and (b) Thickness on Plasmon Energy and Reflectance Magnitude for PtSe₂ Nanoribbons. Results are calculated using the COMSOL Multiphysics wave optics module for a monochromatic, normal incidence, TM polarized plane wave source. The white dotted line in (a) is a fit to equation (3).

S2.2.5. Confirming the Role of PtSe₂ in Plasmon Broadening

We now fix the period of the lossless control device to 300 nm and sweep the width from 110 nm to 225 nm. The TM dispersion (Figure S11) shows the P1 mode, which redshifts minimally and does not broaden with increasing fill factor, unlike the device with actual PtSe₂ (Figure 3d of main manuscript).

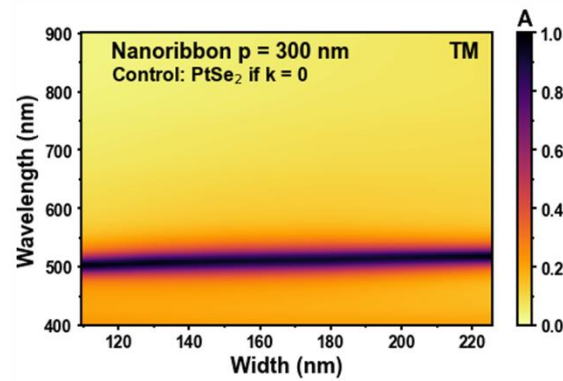
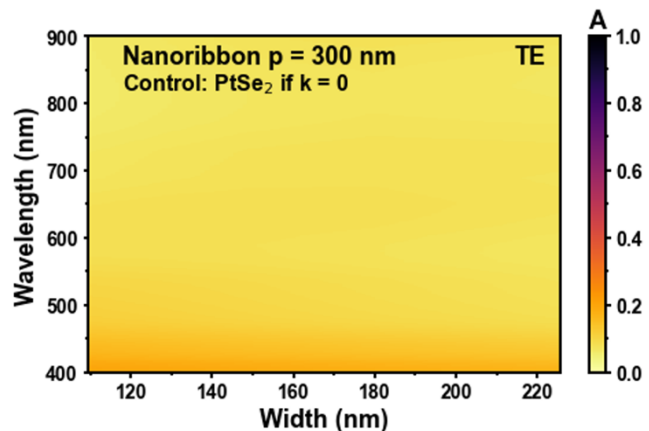


Figure S12. Control $k = 0$ simulation for which the array period is fixed at 300 nm and the width is swept from 110 to 225 nm. Simulated with the COMSOL Multiphysics wave optics module for a monochromatic, normal incidence, TM polarized plane wave source.

S2.2.6. TE Absorbance due to PtSe₂

Figure S13 shows the transverse electric (TE) dispersion. There is less than 10% absorbance from 400 nm to 900 nm; this is the expected amount of loss due to the silver. We can therefore confirm that nearly all absorbance we see in the TE direction in Figure 4 of the main manuscript is due to the large k of PtSe₂.



S3. 2D Metasurface Characterization and Field Profiles

S3.1. More SEM Images of 2D Metasurfaces

In Figure 5b of the main manuscript, SEM images of the nanosquare (NSQ) array device with dimensions ($w = 250$ nm, $p = 300$ nm) and the crossed grating (XG) device with dimensions (100 nm, 300 nm) are shown. NSQ arrays with dimensions (150 nm, 300 nm) and (150 nm, 200 nm) and XGs with dimensions (150 nm, 300 nm) and (200 nm, 300 nm) were also fabricated and characterized (Figure 5c and 5d of main manuscript). SEM images of these other four devices are shown in Figure S14.

Figure S13. Control $k = 0$ simulation for which the array period is fixed at 300 nm and the width is swept from 110 to 225 nm. Simulated with the COMSOL Multiphysics wave optics module for a monochromatic, normal incidence, TE polarized plane wave source.

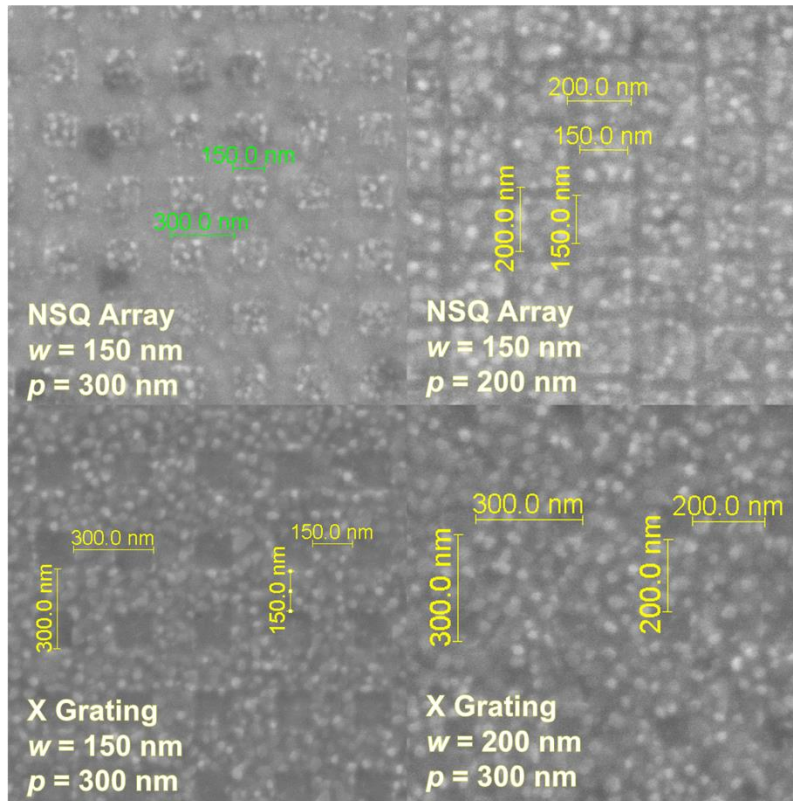


Figure S14. SEM Images of 2D Metasurface Devices not included in Figure 5 of main manuscript. SEM images of nanosquare (NSQ) array devices with width 150 nm, period 300 nm (top left) and width 150 nm, period 200 nm (top right). SEM images of crossed grating (X Grating) devices with width 150 nm, period 300 nm (bottom left) and width 200 nm, period 300 nm (bottom right). Dimensions are measured using the SEM software and overlaid.

S3.2. Field Profiles and Absorption Characteristics of 2D Metasurfaces

The modes of the 2D metasurfaces (2DMSs) were explored using the Lumerical finite difference time domain (FDTD) solver. We simulated the XG and NSQ array structures using normal incident plane waves with linear polarization along the \hat{x} -direction (along one of the axes of periodicity for the array). Given the square lattice and square features, the response to light polarized along the \hat{x}

direction and \hat{y} direction will be identical. Figure S15a shows the calculated $|E|$ field (top) and corresponding P_{abs} (bottom) profiles in the XZ plane ($y = 0$) for an XG device ($w = 150$ nm, $p = 300$ nm) illuminated by an \hat{x} -polarized 550 nm plane wave. The $|E|$ field profile and P_{abs} profile in the XY plane ($z = 8$ nm) for the same device are displayed in Figure S15b. Under this polarization, the modes in the XZ plane can be considered TM modes while the modes in the YZ plane are TE-like. The P_{abs} profile confirms that absorption is dominated by the PtSe₂. The plasmonic response observed in the $|E|$ field profile in Figure S15a is similar to the TM P1 mode of the 1D nanoribbon array. In the XY plane $|E|$ field profile (Figure S15b), TE-like field localization in PtSe₂ is seen when there is confinement in the \hat{y} direction (i.e., for -75 nm $< x < 75$ nm). The power absorption is strongest in the region with TE field enhancement (Figure S15b, bottom). Additionally, slight reduced dependence on fill factor and higher energy resonance (absorbance maximum) – relative to the P1 mode – are both phenomena observed for the TE modes of 1D nanoribbon arrays (Figure 4 in main manuscript). Therefore, while plasmonic field enhancement contributes to absorption, the absorption in the XG geometry is more due to TE-like modes.

Figure S15c shows the calculated E field profile (top) and corresponding P_{abs} profile (bottom) in the XZ plane ($y = 0$) for a NSQ array device ($w = 250$ nm, $p = 300$ nm) illuminated by an \hat{x} -polarized 550 nm plane wave. Figure S15d shows these profiles for the same structure in the XY ($z = 8$ nm). The role of the plasmon resonance is more obvious for this NSQ device. The electric field is localized near the edges of the nanosquare, with little variation in the \hat{y} direction. The regions for which the plasmon localizes and enhances the field are the regions that exhibit the strongest absorption. In contrast to the XG geometry, absorption in the NSQ geometry is dominated by the plasmonic TM-like modes. Again, negligible absorption can be attributed directly to the Ag, but the plasmon resonance assists absorption in the PtSe₂.

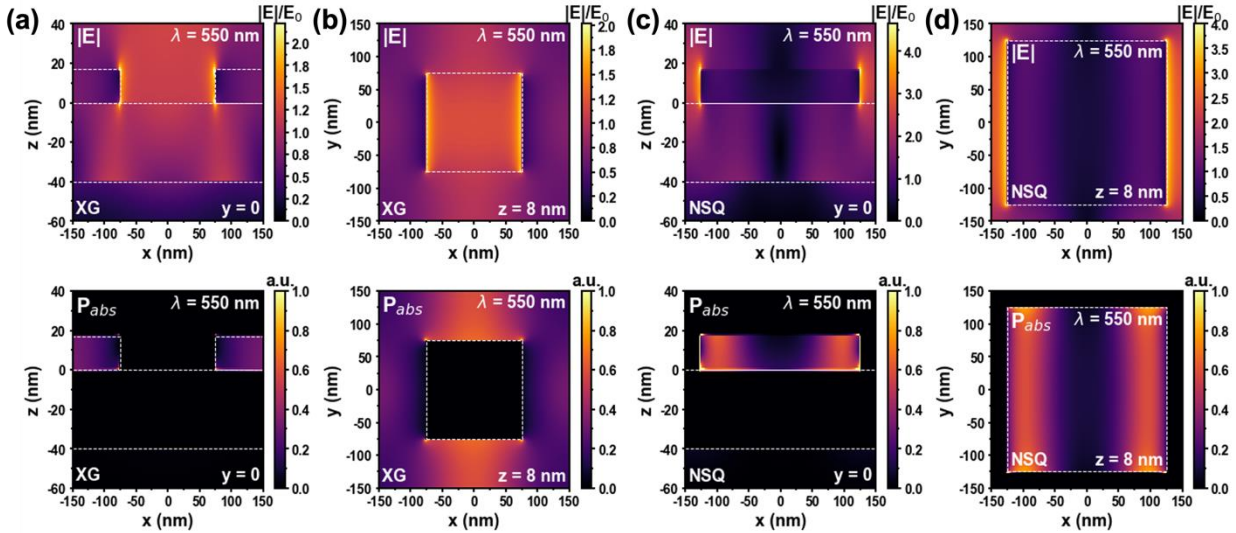


Figure S15. 2DMS Field and Power Absorption Profiles. (a) Simulated electric field magnitude ($|E|$, top) and power absorbed (P_{abs} , bottom) profiles for (a) an X Grating (XG) device ($w = 150$ nm, $p = 300$ nm) in the XZ plane ($y = 0$); (b) the same XG device in the XY plane ($z = 8$ nm); (c) a nanosquare (NSQ) array device ($w = 250$ nm, $p = 300$ nm) in the XZ plane ($y = 0$); and (d) the same NSQ device in the XY plane ($z = 8$ nm). The field profiles were calculated by the Lumerical FDTD solver for a normal incidence plane wave ($\lambda = 550$ nm) polarized with the \vec{E} component

along the \hat{x} direction. Edges of layers and materials are indicated by a white dashed line. The P_{abs} values are normalized to the maximum P_{abs} value for all plots shown to provide a relative comparison.

We further investigate the XG devices within the two regimes of the optical constants for PtSe₂. Figure S16a (top) shows the $|E|$ profile along the YZ plane for an XG device with $w = 150$ nm, $p = 300$ nm illuminated by \hat{x} -polarized light with $\lambda = 425$ nm. Like the nanoribbon TE field profiles (Figure 4b of main manuscript), the electric field is localized and enhanced in the area between the PtSe₂ parallel gratings, resulting in power absorption being localized near the edges of the PtSe₂. For the $\lambda = 900$ nm case (Figure S16b), absorption is again – like the nanoribbon TE case and the XG device for $\lambda = 550$ nm – enhanced by the large refractive index of the PtSe₂, and power is primarily absorbed in the regions where there is confinement in the \hat{y} direction. The similarities to the TE nanoribbon modes further supports the claim that the primary absorption mechanism for XG devices is field enhancement either between the gratings (below 470 nm) or inside the ribbons (above 470 nm).

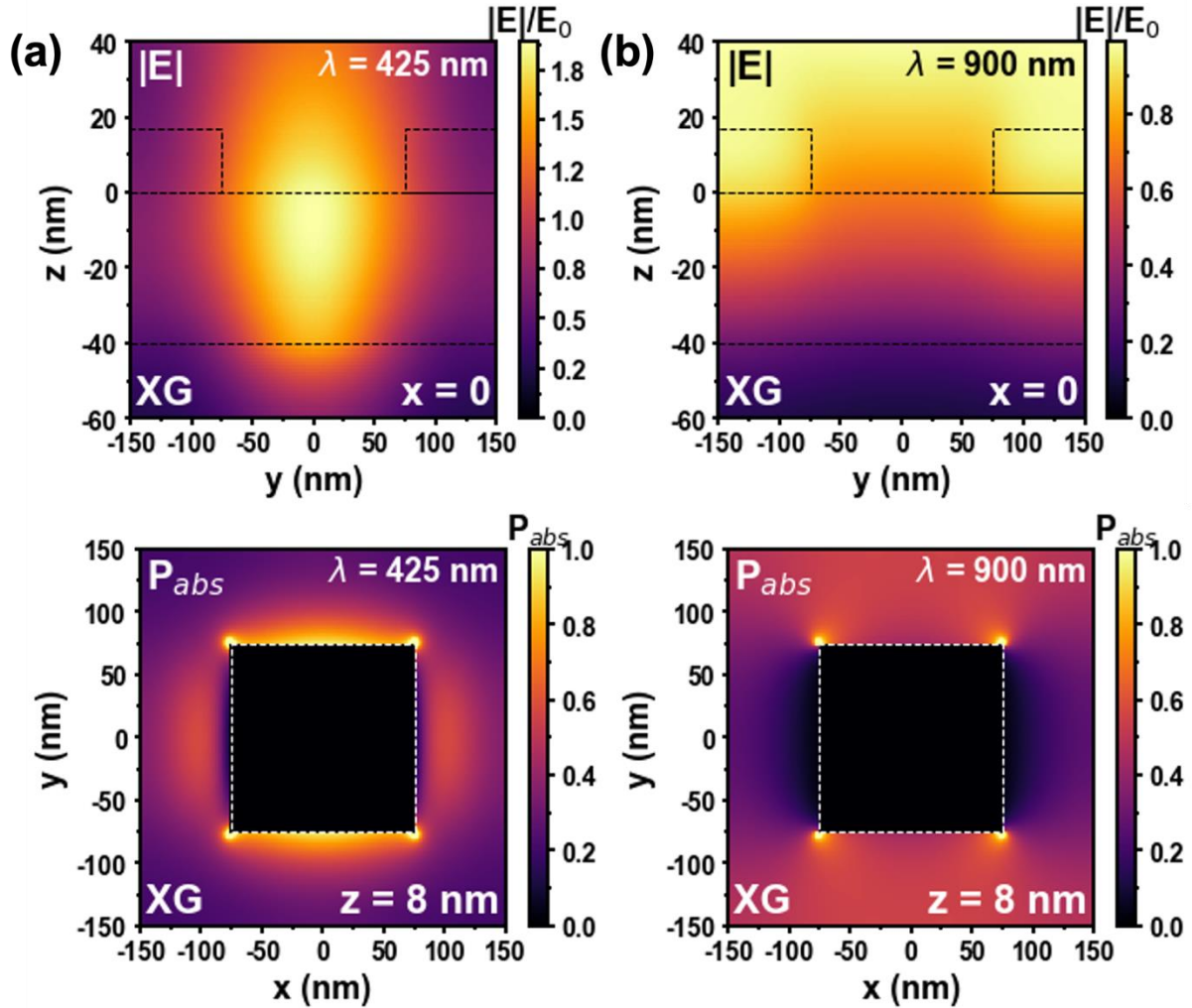


Figure S16. Simulated Field and Power Absorption Profiles for an X Grating Metasurface Illuminated by \hat{x} -Polarized Light with $\lambda = 425$ nm and 900 nm. $|E|$ profile along the YZ plane (top) and P_{abs} profile along the XY plane (bottom) for an XG device with $w = 150$ nm, $p = 300$ nm illuminated by two other wavelengths: $\lambda = 425$ nm (a) and $\lambda = 900$ nm (b).

Similarly, we consider the NSQ array field and power profiles at two more wavelengths. Figure S17 shows the electric field magnitude and P_{abs} profiles for a NSQ array device with $w = 250$ nm, $p = 300$ nm under illumination by an \hat{x} -polarized plane wave with wavelengths $\lambda = 450$ nm and 900 nm, both wavelengths away from the main plasmon resonance. For $\lambda = 450$ nm, there is TE-like localization of the electric field between NSQs in the YZ plane (Figure S17a) and TM-like plasmonic field localization towards the edges of the NSQ in the XZ plane (Figure S17b). The combination of these two modes is observed in the XY plane power profile (Figure S17c).

While the plasmon resonance occurs at approximately 550 nm, the off-resonance plasmon assisted absorption is directly observed at 900 nm for the NSQ. The YZ plane $|E|$ profile indicates plasmonic field enhancement in the center of the NSQ (Figure S17d), resulting in power absorption occurring towards the center (in \hat{x}) of the NSQ (Figures S17e and S17f). The lack of variation in \hat{y} indicates that absorbance is dominated by the TM-like modes at this wavelength. By using plasmons for field enhancement instead of as the primary absorption mechanism, broadband absorption is achieved without the need for resonance multiplexing.

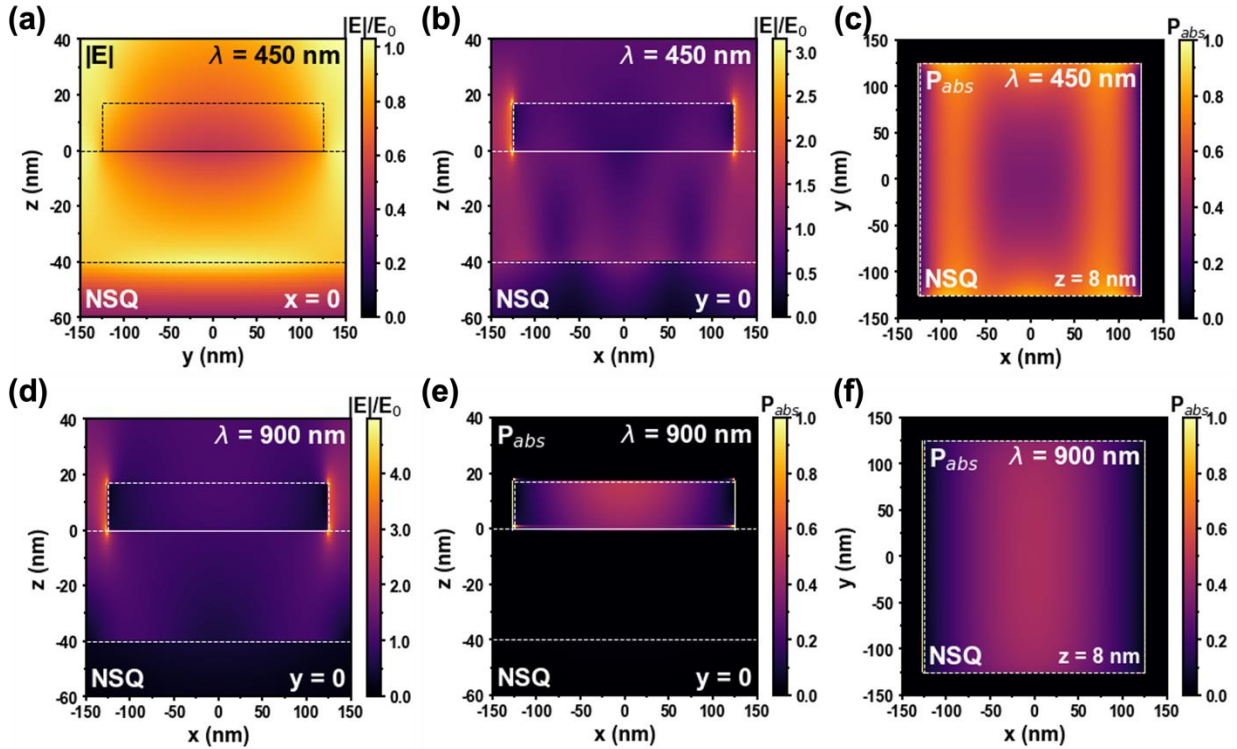


Figure S17. Simulated Field and Power Absorption Profiles for Nanosquare Array Metasurface Illuminated by \hat{x} -Polarized Light with $\lambda = 450$ nm and 900 nm. $|E|$ profile in the YZ plane (a), $|E|$ profile in the XZ plane (b), and P_{abs} profile in the XY plane (c) for a NSQ array device with $w = 250$ nm, $p = 300$ nm for $\lambda = 450$ nm. $|E|$ profile in the XZ plane (d), P_{abs} profile in the XZ plane (e), and P_{abs} profile in the XY plane (f) for the same NSQ array device for $\lambda = 900$ nm.

S3.3. Simulated Absorbance Dispersion for 2DMSs

Using the Lumerical FDTD solver, we simulated the 2DMSs shown in Figure 5a of the main manuscript for \hat{x} -polarized plane waves at normal incidence using a broadband source (400 nm to

900 nm). Figure S18a is a plot of A in an XG device as a function of wavelength and p for a fixed w of 150 nm. Figure S18b shows A in an XG device as a function of wavelength and w for a fixed $p = 300$ nm. Similarly, Figures S18c and S18d show A spectra as a function of period (fixed $w = 150$ nm) and width (fixed $p = 300$ nm) for a NSQ array. The X Grating devices exhibit significantly less dependence on fill factor than the NSQ arrays. For the NSQ devices, there are distinct plasmonic resonances at low fill factors that broaden with increasing fill factor, resulting in broadband absorption. This is consistent with what is observed for the TM modes of the nanoribbon arrays.

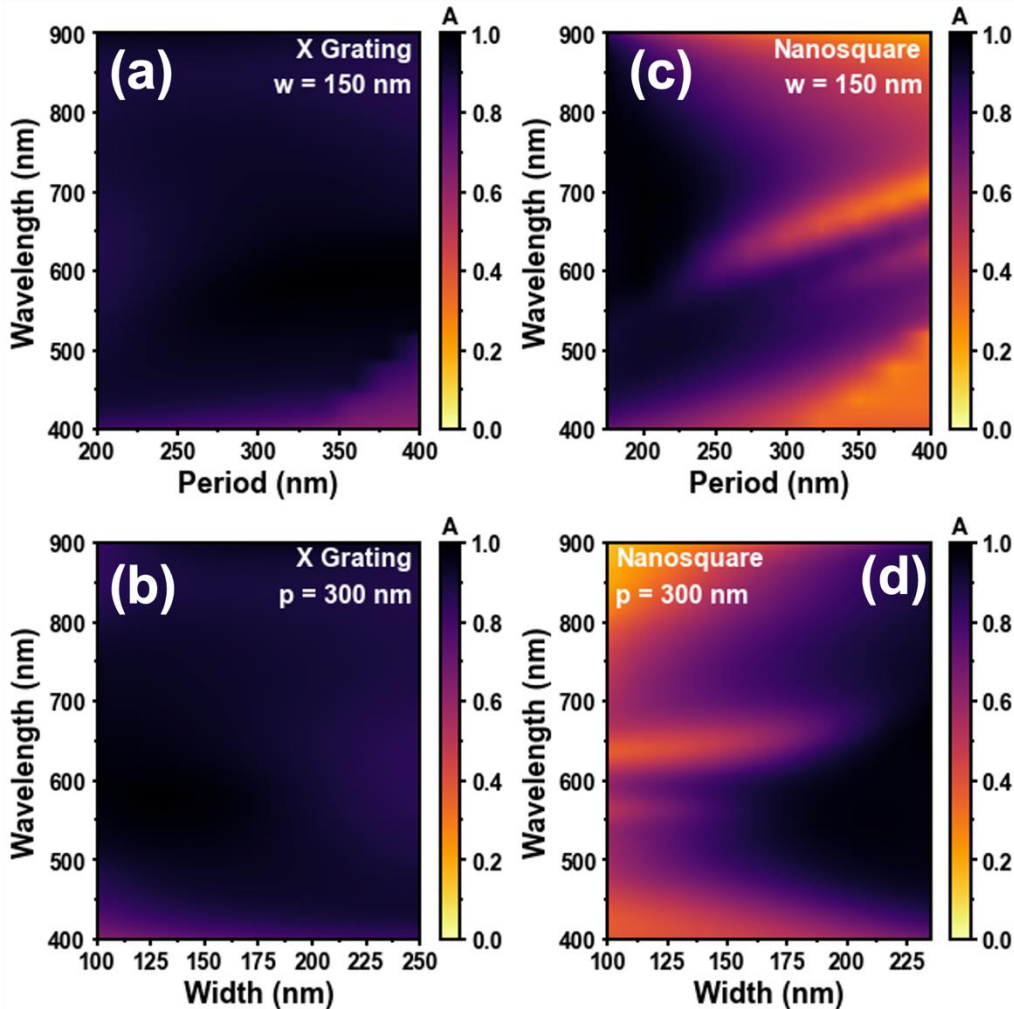


Figure S18. Dispersions of Absorbance Spectra for 2D Metasurface Devices. (a) Absorbance as a function of wavelength and period for an X Grating device with fixed $w = 150$ nm. (b) Absorbance as a function of wavelength and width for an X Grating device with fixed $p = 300$ nm. (c) Absorbance as a function of wavelength and period for an NSQ Array device with fixed $w = 150$ nm. (d) Absorbance as a function of wavelength and width for a NSQ array device with fixed $p = 300$ nm.

References

- [1] F. Ding, Y. Yang, R. A. Deshpande, S. I. Bozhevolnyi, *Nanophotonics* **2018**, 7, 1129.
- [2] W. L. Barnes, A. Dereux, T. W. Ebbesen, *Nature* **2003**, 424, 824.

Table 1. Fit parameters for PtSe₂ grown at 550°C before and after transfer

PARAMETER	AS GROWN	POST-TRANSFER
MSE	2.824	2.93
Roughness (nm)	2.0±0.542	1.162
Thickness (nm)	8.3±0.439	17.11
ϵ_{∞}	2.041±0.0405	1.544
A_{UV}	15.5362±1.18301	20.4668
E_{UV} (eV)	6.548±0.0406	6.750
A_{IR}	1.0517±0.07634	0
A_1	16.009524±1.3807628	7.810893
Γ_1 (eV)	1.7411±0.02524	1.1840
E_1 (eV)	2.737±0.005758	2.779
A_2	30.05389±2.0949219	10.837
Γ_2 (eV)	0.6637±0.00412	0.5682
E_2 (eV)	1.453±0.002186	1.480
A_3	11.939459±0.9658847	4.740844
Γ_3 (eV)	1.166±0.04441	1.0109
E_3 (eV)	1.945±0.005159	1.942
A_4	3.207054±0.1500741	1.536796
Γ_4 (eV)	2.4721±0.10155	0.4878
E_4 (eV)	5.748±0.0138	11.040

Table 2. Optical constants for transferred PtSe₂ grown at 550°C for 240 nm to 900 nm.

Wavelength (nm)	n	k	ϵ'	ϵ''
240	0.805143	0.595336	0.2938303	0.95866123
250	0.737805	0.760954	-0.0346948	1.12287133
260	0.711644	0.920726	-0.3412992	1.31045827
270	0.712898	1.068935	-0.6343985	1.52408325
280	0.732459	1.205868	-0.9176214	1.76649774
290	0.765277	1.333163	-1.1916747	2.04047796
300	0.808623	1.452258	-1.4551821	2.34865844
310	0.860991	1.56409	-1.705072	2.69333483
320	0.921505	1.669127	-1.9368135	3.07621775
330	0.989585	1.767438	-2.1445586	3.49806027
340	1.064755	1.858784	-2.3213747	3.95829912
350	1.146506	1.94269	-2.4595684	4.45461148

360	1.234205	2.018519	-2.551157	4.98253248
370	1.327026	2.085558	-2.5885542	5.53517938
380	1.423907	2.143112	-2.5654179	6.10318436
390	1.523543	2.190606	-2.4775714	6.67496487
400	1.624411	2.227693	-2.323905	7.23737803
410	1.724839	2.254339	-2.1069748	7.77674365
420	1.823108	2.270894	-1.8332368	8.28017004
430	1.917572	2.278109	-1.5126982	8.73687606
440	2.006792	2.277113	-1.1580295	9.1393843
450	2.089642	2.26934	-0.7833003	9.48421635
460	2.16539	2.256419	-0.4025129	9.77205428
470	2.233726	2.240051	-0.0282966	10.0073203
480	2.294754	2.221883	0.32913185	10.1973498
490	2.348943	2.203408	0.6625264	10.3513596
500	2.397054	2.185875	0.96781836	10.4793208
510	2.440051	2.17025	1.24386382	10.5910414
520	2.479012	2.157181	1.49207063	10.6953552
530	2.515043	2.14701	1.71578935	10.7996449
540	2.549199	2.139789	1.91971858	10.909496
550	2.582414	2.135319	2.10927484	11.0285554
560	2.615452	2.133209	2.29000853	11.1586115
570	2.648867	2.132934	2.46708894	11.299717
580	2.682988	2.133914	2.64483565	11.4505313
590	2.717922	2.135579	2.82640233	11.6086743
600	2.753585	2.137444	3.0135635	11.7712675
610	2.789745	2.13916	3.20667166	11.9354218
620	2.826091	2.14055	3.40483604	12.0987782
630	2.862296	2.141622	3.6061936	12.2599122
640	2.898093	2.142554	3.80840539	12.4186415
650	2.933328	2.143661	4.00913067	12.5761217
660	2.968009	2.145343	4.20658084	12.7347947
670	3.002323	2.148021	4.39994918	12.8981057
680	3.036644	2.152072	4.58979289	13.0701531
690	3.071511	2.15777	4.77820845	13.2552286
700	3.107592	2.165226	4.96892441	13.457278
710	3.145636	2.174352	5.16721922	13.6794399

720	3.186408	2.184833	5.3797007	13.9235387
730	3.230625	2.196118	5.61400362	14.1896674
740	3.278883	2.207432	5.87831769	14.4758225
750	3.331591	2.217806	6.18083514	14.777645
760	3.388913	2.226133	6.52906319	15.0883421
770	3.450721	2.231233	6.92907472	15.3987251
780	3.516577	2.231942	7.38474871	15.6975918
790	3.585735	2.2272	7.89707565	15.972298
800	3.65718	2.216142	8.46368019	16.2096604
810	3.729686	2.198174	9.07858872	16.3969976
820	3.801909	2.17302	9.73249612	16.5232486
830	3.872478	2.140748	10.4132839	16.5799991
840	3.940102	2.101752	11.1070423	16.5622345
850	4.00365	2.056709	11.7991614	16.468686
860	4.062219	2.00651	12.4755408	16.3017661
870	4.115167	1.952179	13.1235966	16.0670852
880	4.162121	1.89479	13.7330221	15.7726905
890	4.202956	1.835399	14.2961496	15.4282025
900	4.237761	1.774984	14.8080501	15.0439159

Table 3. Optical constants for as-grown PtSe₂ grown at 550°C for 210 nm to 2500 nm.

Wavelength (nm)	<i>n</i>	<i>k</i>	ϵ'	ϵ''
210	1.422846	1.537909	-0.340673	4.376415
211	1.420147	1.552269	-0.392721	4.408903
212	1.4182	1.565147	-0.438393	4.439384
213	1.416832	1.576724	-0.478646	4.467905
214	1.415901	1.587159	-0.514297	4.49452
215	1.415293	1.596589	-0.546041	4.519281
216	1.414912	1.605134	-0.574479	4.542249
217	1.414681	1.612902	-0.600131	4.563482
218	1.414532	1.619985	-0.623451	4.583044
219	1.414413	1.626469	-0.644838	4.600999
220	1.414278	1.632428	-0.66464	4.617414
221	1.414089	1.63793	-0.683168	4.632359
222	1.413815	1.643036	-0.700694	4.645901
223	1.413431	1.647802	-0.717463	4.658111
224	1.412916	1.652278	-0.733692	4.669059

225	1.412251	1.65651	-0.749573	4.678818
226	1.411425	1.660542	-0.765279	4.687459
227	1.410425	1.664411	-0.780966	4.695054
228	1.409244	1.668154	-0.796769	4.701673
229	1.407876	1.671805	-0.812815	4.707389
230	1.406318	1.675393	-0.829211	4.712271
231	1.404567	1.678948	-0.846058	4.71639
232	1.402623	1.682496	-0.863441	4.719815
233	1.400487	1.686062	-0.88144	4.722614
234	1.398161	1.689668	-0.900123	4.724854
235	1.395649	1.693336	-0.91955	4.726603
236	1.392954	1.697085	-0.939776	4.727923
237	1.390083	1.700935	-0.960848	4.72888
238	1.387041	1.704901	-0.982805	4.729535
239	1.383835	1.709	-1.005682	4.729949
240	1.380473	1.713247	-1.029511	4.730182
241	1.376962	1.717655	-1.054314	4.73029
242	1.373311	1.722236	-1.080114	4.730332
243	1.369529	1.727002	-1.106925	4.730361
244	1.365626	1.731964	-1.134762	4.73043
245	1.361611	1.73713	-1.163634	4.730591
246	1.357495	1.742509	-1.193546	4.730894
247	1.353286	1.74811	-1.224503	4.731386
248	1.348997	1.753938	-1.256505	4.732115
249	1.344638	1.76	-1.289551	4.733125
250	1.340218	1.766302	-1.323637	4.73446
251	1.33575	1.772847	-1.358756	4.736162
252	1.331245	1.779639	-1.394902	4.73827
253	1.326712	1.786681	-1.432065	4.740824
254	1.322164	1.793976	-1.470234	4.74386
255	1.31761	1.801525	-1.509397	4.747414
256	1.313062	1.809329	-1.54954	4.751521
257	1.30853	1.817388	-1.59065	4.756212
258	1.304024	1.825702	-1.63271	4.76152
259	1.299556	1.834271	-1.675704	4.767474
260	1.295134	1.843092	-1.719614	4.774103
261	1.29077	1.852163	-1.764423	4.781434
262	1.286472	1.861484	-1.810111	4.789493
263	1.28225	1.871049	-1.856661	4.798305
264	1.278112	1.880857	-1.904051	4.807893

265	1.274069	1.890903	-1.952262	4.818281
266	1.270127	1.901183	-2.001274	4.829489
267	1.266296	1.911693	-2.051065	4.841538
268	1.262582	1.922428	-2.101614	4.854447
269	1.258994	1.933383	-2.152901	4.868235
270	1.255538	1.944552	-2.204904	4.882918
271	1.252221	1.95593	-2.257601	4.898514
272	1.24905	1.96751	-2.310971	4.915037
273	1.246029	1.979288	-2.364992	4.932503
274	1.243166	1.991257	-2.419643	4.950925
275	1.240464	2.00341	-2.474901	4.970316
276	1.237929	2.015742	-2.530746	4.99069
277	1.235565	2.028244	-2.587155	5.012056
278	1.233377	2.040913	-2.644107	5.034428
279	1.231367	2.053739	-2.70158	5.057814
280	1.22954	2.066718	-2.759553	5.082224
281	1.227898	2.079841	-2.818006	5.107668
282	1.226445	2.093104	-2.876916	5.134155
283	1.225183	2.106498	-2.936262	5.161692
284	1.224113	2.120018	-2.996025	5.190286
285	1.223239	2.133658	-3.056182	5.219946
286	1.222561	2.14741	-3.116714	5.250677
287	1.22208	2.161268	-3.1776	5.282485
288	1.221798	2.175226	-3.238819	5.315377
289	1.221717	2.189279	-3.300352	5.349357
290	1.221835	2.20342	-3.362179	5.384431
291	1.222154	2.217643	-3.424278	5.420603
292	1.222675	2.231942	-3.486633	5.457878
293	1.223396	2.246312	-3.549221	5.496259
294	1.224319	2.260748	-3.612024	5.53575
295	1.225442	2.275243	-3.675023	5.576355
296	1.226765	2.289793	-3.738198	5.618076
297	1.228289	2.304392	-3.801531	5.660917
298	1.230011	2.319036	-3.865002	5.704879
299	1.231932	2.33372	-3.928592	5.749966
300	1.23405	2.348438	-3.992284	5.796179
301	1.236364	2.363187	-4.056058	5.84352
302	1.238874	2.377962	-4.119896	5.89199
303	1.241578	2.392759	-4.18378	5.941592
304	1.244474	2.407573	-4.247691	5.992326

305	1.247563	2.4224	-4.311611	6.044194
306	1.250841	2.437238	-4.375523	6.097196
307	1.254309	2.45208	-4.439406	6.151332
308	1.257964	2.466925	-4.503245	6.206604
309	1.261805	2.481768	-4.56702	6.263012
310	1.26583	2.496606	-4.630714	6.320556
311	1.270038	2.511435	-4.69431	6.379235
312	1.274427	2.526253	-4.757788	6.43905
313	1.278996	2.541055	-4.821132	6.5
314	1.283743	2.55584	-4.884323	6.562085
315	1.288667	2.570604	-4.947343	6.625304
316	1.293765	2.585344	-5.010176	6.689655
317	1.299037	2.600057	-5.072803	6.755139
318	1.30448	2.614741	-5.135205	6.821754
319	1.310093	2.629393	-5.197366	6.889497
320	1.315874	2.644011	-5.259268	6.958368
321	1.321822	2.658591	-5.320892	7.028366
322	1.327935	2.673131	-5.382221	7.099487
323	1.334211	2.68763	-5.443237	7.17173
324	1.340649	2.702084	-5.503922	7.245092
325	1.347247	2.716492	-5.564257	7.319571
326	1.354003	2.730851	-5.624225	7.395164
327	1.360917	2.74516	-5.683808	7.471868
328	1.367985	2.759415	-5.742988	7.549679
329	1.375208	2.773615	-5.801746	7.628595
330	1.382582	2.787759	-5.860065	7.708612
331	1.390108	2.801843	-5.917925	7.789725
332	1.397782	2.815866	-5.975308	7.871932
333	1.405603	2.829826	-6.032197	7.955225
334	1.413571	2.843722	-6.088573	8.039603
335	1.421682	2.857551	-6.144417	8.12506
336	1.429937	2.871312	-6.199711	8.211589
337	1.438333	2.885002	-6.254436	8.299187
338	1.446869	2.898621	-6.308573	8.387846
339	1.455542	2.912166	-6.362104	8.477561
340	1.464353	2.925635	-6.41501	8.568326
341	1.473299	2.939028	-6.467273	8.660132
342	1.482379	2.952341	-6.518873	8.752975
343	1.49159	2.965575	-6.569792	8.846847
344	1.500933	2.978726	-6.62001	8.941737

345	1.510405	2.991794	-6.66951	9.037642
346	1.520004	3.004777	-6.718271	9.134548
347	1.52973	3.017673	-6.766276	9.23245
348	1.53958	3.030481	-6.813505	9.331338
349	1.549554	3.043199	-6.85994	9.431202
350	1.559649	3.055825	-6.905561	9.532031
351	1.569865	3.068359	-6.95035	9.633817
352	1.580199	3.080798	-6.994288	9.736547
353	1.59065	3.093141	-7.037356	9.840209
354	1.601216	3.105387	-7.079536	9.944794
355	1.611897	3.117534	-7.120809	10.050288
356	1.62269	3.129581	-7.161156	10.156679
357	1.633594	3.141526	-7.200559	10.263954
358	1.644606	3.153368	-7.238999	10.372099
359	1.655727	3.165105	-7.276459	10.481101
360	1.666954	3.176736	-7.31292	10.590944
361	1.678284	3.18826	-7.348365	10.701614
362	1.689718	3.199675	-7.382775	10.813096
363	1.701252	3.21098	-7.416133	10.925374
364	1.712886	3.222173	-7.448421	11.038431
365	1.724617	3.233254	-7.479623	11.152251
366	1.736445	3.24422	-7.509722	11.266816
367	1.748366	3.25507	-7.5387	11.38211
368	1.76038	3.265804	-7.56654	11.498111
369	1.772484	3.27642	-7.593228	11.614803
370	1.784677	3.286916	-7.618747	11.732166
371	1.796957	3.297292	-7.643082	11.850181
372	1.809321	3.307546	-7.666216	11.968826
373	1.821769	3.317677	-7.688136	12.088082
374	1.834298	3.327683	-7.708826	12.207927
375	1.846907	3.337564	-7.728272	12.328339
376	1.859592	3.347319	-7.746461	12.449296
377	1.872353	3.356946	-7.76338	12.570776
378	1.885187	3.366444	-7.779016	12.692755
379	1.898093	3.375813	-7.793355	12.815209
380	1.911067	3.38505	-7.806386	12.938116
381	1.924109	3.394156	-7.818098	13.06145
382	1.937216	3.403128	-7.828479	13.185186
383	1.950385	3.411968	-7.83752	13.3093
384	1.963615	3.420672	-7.84521	13.433765

385	1.976904	3.42924	-7.851541	13.558556
386	1.990248	3.437672	-7.856503	13.683644
387	2.003647	3.445967	-7.860089	13.809006
388	2.017098	3.454124	-7.86229	13.934611
389	2.030598	3.462142	-7.863101	14.060435
390	2.044145	3.470021	-7.862516	14.186448
391	2.057736	3.477759	-7.860528	14.312622
392	2.071371	3.485357	-7.857134	14.43893
393	2.085045	3.492813	-7.852328	14.565341
394	2.098757	3.500127	-7.846109	14.691829
395	2.112504	3.507299	-7.838473	14.818362
396	2.126283	3.514328	-7.829419	14.944913
397	2.140093	3.521214	-7.818945	15.071451
398	2.153931	3.527956	-7.807052	15.197948
399	2.167794	3.534554	-7.79374	15.324372
400	2.18168	3.541008	-7.77901	15.450695
401	2.195587	3.547318	-7.762865	15.576887
402	2.209511	3.553483	-7.745307	15.702918
403	2.22345	3.559504	-7.726341	15.828758
404	2.237402	3.56538	-7.70597	15.954376
405	2.251364	3.571112	-7.684202	16.079744
406	2.265333	3.576699	-7.661041	16.20483
407	2.279308	3.582142	-7.636495	16.329607
408	2.293285	3.58744	-7.610573	16.454044
409	2.307261	3.592595	-7.583282	16.57811
410	2.321235	3.597606	-7.554633	16.701778
411	2.335204	3.602473	-7.524636	16.82502
412	2.349164	3.607198	-7.493303	16.947803
413	2.363115	3.61178	-7.460645	17.070103
414	2.377052	3.616221	-7.426676	17.191889
415	2.390973	3.62052	-7.39141	17.313133
416	2.404877	3.624678	-7.354862	17.433811
417	2.41876	3.628697	-7.317046	17.553892
418	2.432619	3.632577	-7.277978	17.673351
419	2.446453	3.636318	-7.237677	17.792162
420	2.460258	3.639922	-7.19616	17.910299
421	2.474034	3.643389	-7.153445	18.027737
422	2.487776	3.646722	-7.109551	18.144449
423	2.501482	3.649919	-7.064499	18.260414
424	2.515151	3.652984	-7.018309	18.375608

425	2.528779	3.655916	-6.971003	18.490009
426	2.542365	3.658718	-6.922601	18.603592
427	2.555905	3.661391	-6.873128	18.716335
428	2.569399	3.663935	-6.822606	18.82822
429	2.582843	3.666352	-6.77106	18.939228
430	2.596236	3.668645	-6.718512	19.049334
431	2.609575	3.670813	-6.664989	19.158524
432	2.622858	3.67286	-6.610515	19.266777
433	2.636083	3.674786	-6.555117	19.374079
434	2.649248	3.676593	-6.498821	19.48041
435	2.662351	3.678283	-6.441653	19.585756
436	2.67539	3.679857	-6.383641	19.690104
437	2.688363	3.681319	-6.324812	19.793438
438	2.701268	3.682668	-6.265195	19.895746
439	2.714104	3.683908	-6.204816	19.997015
440	2.726868	3.68504	-6.143705	20.097233
441	2.73956	3.686065	-6.081891	20.196392
442	2.752177	3.686987	-6.019401	20.294481
443	2.764717	3.687808	-5.956265	20.391491
444	2.77718	3.688529	-5.892513	20.487415
445	2.789564	3.689152	-5.828174	20.582247
446	2.801867	3.689679	-5.763276	20.675978
447	2.814088	3.690114	-5.697849	20.768606
448	2.826225	3.690457	-5.631923	20.860125
449	2.838278	3.690711	-5.565527	20.950533
450	2.850246	3.69088	-5.498691	21.039827
451	2.862126	3.690963	-5.431444	21.128004
452	2.873919	3.690965	-5.363814	21.215067
453	2.885623	3.690887	-5.295831	21.301014
454	2.897236	3.690732	-5.227525	21.385845
455	2.908759	3.690502	-5.158922	21.469563
456	2.920191	3.690199	-5.090053	21.552172
457	2.93153	3.689826	-5.020944	21.633675
458	2.942777	3.689385	-4.951625	21.714073
459	2.95393	3.688879	-4.882122	21.793377
460	2.964989	3.688309	-4.812463	21.87159
461	2.975953	3.687679	-4.742675	21.948717
462	2.986823	3.68699	-4.672784	22.024769
463	2.997597	3.686245	-4.602816	22.099752
464	3.008275	3.685447	-4.532798	22.173676

465	3.018858	3.684597	-4.462753	22.24655
466	3.029345	3.683699	-4.392708	22.318384
467	3.039735	3.682754	-4.322687	22.389191
468	3.050029	3.681765	-4.252712	22.458979
469	3.060227	3.680734	-4.182808	22.527763
470	3.070329	3.679663	-4.112998	22.595556
471	3.080335	3.678555	-4.043302	22.662369
472	3.090246	3.677413	-3.973743	22.728216
473	3.10006	3.676237	-3.904342	22.793114
474	3.10978	3.675031	-3.83512	22.857077
475	3.119405	3.673797	-3.766096	22.920116
476	3.128935	3.672536	-3.697289	22.982254
477	3.138371	3.671252	-3.628719	23.043503
478	3.147714	3.669946	-3.560402	23.103878
479	3.156963	3.66862	-3.492356	23.163399
480	3.166121	3.667277	-3.424599	23.222082
481	3.175186	3.665918	-3.357145	23.279945
482	3.184161	3.664545	-3.29001	23.337006
483	3.193046	3.663161	-3.22321	23.393282
484	3.201841	3.661767	-3.156758	23.448793
485	3.210547	3.660366	-3.090667	23.503555
486	3.219166	3.658959	-3.02495	23.55759
487	3.227698	3.657547	-2.959619	23.610916
488	3.236144	3.656134	-2.894686	23.663551
489	3.244505	3.65472	-2.830162	23.715515
490	3.252783	3.653307	-2.766056	23.766827
491	3.260977	3.651897	-2.702378	23.817507
492	3.26909	3.650491	-2.639136	23.867573
493	3.277123	3.649092	-2.576339	23.917046
494	3.285076	3.647701	-2.513995	23.965946
495	3.292951	3.646318	-2.452111	24.014292
496	3.300749	3.644946	-2.390691	24.062103
497	3.308471	3.643586	-2.329743	24.109398
498	3.316118	3.64224	-2.269271	24.156199
499	3.323693	3.640908	-2.20928	24.202522
500	3.331195	3.639593	-2.149774	24.248388
501	3.338627	3.638294	-2.090756	24.293818
502	3.34599	3.637015	-2.032228	24.338827
503	3.353284	3.635754	-1.974193	24.383438
504	3.360513	3.634515	-1.916653	24.427666

505	3.367676	3.633297	-1.859608	24.471531
506	3.374775	3.632102	-1.803059	24.515053
507	3.381812	3.630931	-1.747007	24.558249
508	3.388788	3.629784	-1.69145	24.601135
509	3.395704	3.628663	-1.636388	24.643732
510	3.402563	3.627568	-1.581819	24.686056
511	3.409364	3.626501	-1.527742	24.728123
512	3.416111	3.625461	-1.474155	24.769953
513	3.422803	3.62445	-1.421053	24.811558
514	3.429444	3.623468	-1.368436	24.852959
515	3.436033	3.622516	-1.316297	24.894171
516	3.442573	3.621594	-1.264635	24.935207
517	3.449065	3.620704	-1.213445	24.976088
518	3.455511	3.619844	-1.162721	25.016823
519	3.461911	3.619017	-1.112459	25.05743
520	3.468267	3.618222	-1.062653	25.097923
521	3.474582	3.61746	-1.013298	25.138319
522	3.480855	3.61673	-0.964388	25.178627
523	3.487089	3.616034	-0.915916	25.218864
524	3.493284	3.615371	-0.867876	25.259041
525	3.499443	3.614743	-0.820261	25.299173
526	3.505567	3.614147	-0.773063	25.339272
527	3.511656	3.613586	-0.726276	25.379347
528	3.517713	3.61306	-0.679892	25.419415
529	3.523739	3.612567	-0.633904	25.459482
530	3.529734	3.612108	-0.588302	25.499563
531	3.535701	3.611684	-0.543079	25.539667
532	3.54164	3.611294	-0.498227	25.579805
533	3.547553	3.610938	-0.453737	25.619986
534	3.553441	3.610615	-0.409601	25.660219
535	3.559305	3.610327	-0.36581	25.700516
536	3.565147	3.610073	-0.322354	25.740883
537	3.570967	3.609852	-0.279225	25.78133
538	3.576767	3.609665	-0.236415	25.821863
539	3.582549	3.60951	-0.193912	25.862494
540	3.588312	3.609389	-0.15171	25.903225
541	3.594058	3.6093	-0.109797	25.944067
542	3.599788	3.609244	-0.068165	25.985023
543	3.605504	3.609219	-0.026804	26.026104
544	3.611206	3.609226	0.014294	26.067312

545	3.616895	3.609264	0.05514	26.108656
546	3.622572	3.609333	0.095743	26.150137
547	3.628238	3.609432	0.136112	26.191763
548	3.633895	3.609562	0.176257	26.233538
549	3.639543	3.609721	0.216187	26.275467
550	3.645182	3.609909	0.255912	26.317553
551	3.650815	3.610126	0.29544	26.359798
552	3.65644	3.61037	0.334781	26.402208
553	3.66206	3.610643	0.373944	26.444784
554	3.667675	3.610942	0.412939	26.487532
555	3.673287	3.611269	0.451773	26.530449
556	3.678894	3.611621	0.490457	26.573544
557	3.684499	3.611999	0.528999	26.616812
558	3.690102	3.612401	0.567407	26.660259
559	3.695703	3.612829	0.605691	26.703884
560	3.701304	3.61328	0.643859	26.74769
561	3.706904	3.613754	0.681919	26.791677
562	3.712504	3.614251	0.71988	26.835846
563	3.718106	3.61477	0.757749	26.880196
564	3.723709	3.615311	0.795534	26.924728
565	3.729313	3.615872	0.833244	26.96944
566	3.73492	3.616454	0.870886	27.014336
567	3.74053	3.617056	0.908468	27.059412
568	3.746142	3.617677	0.945996	27.104668
569	3.751759	3.618317	0.983478	27.150103
570	3.757379	3.618974	1.020922	27.195715
571	3.763003	3.619649	1.058333	27.241505
572	3.768632	3.620341	1.095718	27.28747
573	3.774266	3.62105	1.133085	27.333609
574	3.779905	3.621773	1.170438	27.379919
575	3.785549	3.622513	1.207785	27.426399
576	3.791199	3.623266	1.24513	27.473047
577	3.796854	3.624034	1.282481	27.519859
578	3.802516	3.624815	1.319842	27.566837
579	3.808184	3.62561	1.357218	27.613976
580	3.813858	3.626416	1.394615	27.66127
581	3.819538	3.627235	1.432037	27.708723
582	3.825225	3.628065	1.469489	27.756329
583	3.830918	3.628906	1.506976	27.804085
584	3.836618	3.629757	1.544502	27.851988

585	3.842325	3.630619	1.582071	27.900036
586	3.848039	3.63149	1.619687	27.948225
587	3.853759	3.63237	1.657353	27.996555
588	3.859487	3.633258	1.695073	28.045019
589	3.865221	3.634155	1.732851	28.093616
590	3.870961	3.635059	1.770688	28.142344
591	3.876709	3.635971	1.808589	28.191198
592	3.882463	3.636889	1.846556	28.240177
593	3.888224	3.637815	1.884591	28.289276
594	3.893991	3.638746	1.922696	28.338491
595	3.899765	3.639683	1.960874	28.387823
596	3.905546	3.640626	1.999127	28.437265
597	3.911332	3.641575	2.037456	28.486816
598	3.917125	3.642528	2.075863	28.536474
599	3.922924	3.643485	2.11435	28.586235
600	3.928729	3.644448	2.152916	28.636095
601	3.93454	3.645414	2.191565	28.686052
602	3.940357	3.646384	2.230296	28.736105
603	3.946179	3.647358	2.269109	28.786251
604	3.952006	3.648335	2.308007	28.836485
605	3.957839	3.649315	2.346988	28.886808
606	3.963677	3.650299	2.386055	28.937216
607	3.96952	3.651286	2.425205	28.987705
608	3.975368	3.652275	2.46444	29.038275
609	3.981221	3.653267	2.503759	29.088924
610	3.987078	3.654262	2.543162	29.13965
611	3.992939	3.655259	2.582649	29.190453
612	3.998805	3.656258	2.622219	29.241327
613	4.004675	3.65726	2.661872	29.292273
614	4.010549	3.658264	2.701607	29.343288
615	4.016426	3.65927	2.741422	29.394375
616	4.022307	3.660278	2.781318	29.445528
617	4.028192	3.661289	2.821293	29.49675
618	4.03408	3.662302	2.861346	29.548037
619	4.039971	3.663317	2.901477	29.599388
620	4.045866	3.664334	2.941683	29.650806
621	4.051763	3.665354	2.981964	29.702288
622	4.057663	3.666376	3.022319	29.753834
623	4.063566	3.6674	3.062745	29.805445
624	4.069471	3.668427	3.103243	29.857119

625	4.07538	3.669456	3.143809	29.908857
626	4.08129	3.670489	3.184444	29.960661
627	4.087204	3.671524	3.225145	30.012531
628	4.093119	3.672562	3.265912	30.064466
629	4.099037	3.673603	3.306742	30.11647
630	4.104957	3.674648	3.347634	30.168541
631	4.110879	3.675696	3.388588	30.22068
632	4.116804	3.676747	3.429601	30.272892
633	4.12273	3.677803	3.470672	30.325174
634	4.128659	3.678862	3.5118	30.377533
635	4.13459	3.679925	3.552984	30.429964
636	4.140523	3.680993	3.594222	30.482475
637	4.146459	3.682065	3.635513	30.535065
638	4.152397	3.683143	3.676856	30.587738
639	4.158337	3.684225	3.718251	30.640495
640	4.164279	3.685312	3.759695	30.69334
641	4.170225	3.686405	3.801189	30.746273
642	4.176172	3.687504	3.842731	30.799301
643	4.182123	3.688608	3.884321	30.852425
644	4.188076	3.689719	3.925958	30.905647
645	4.194033	3.690836	3.967641	30.958971
646	4.199992	3.691959	4.009371	31.012403
647	4.205956	3.69309	4.051147	31.065943
648	4.211922	3.694228	4.092968	31.119596
649	4.217892	3.695373	4.134835	31.173368
650	4.223866	3.696525	4.176748	31.227259
651	4.229845	3.697686	4.218708	31.281277
652	4.235828	3.698854	4.260713	31.335423
653	4.241816	3.700032	4.302765	31.389702
654	4.247808	3.701217	4.344866	31.44412
655	4.253806	3.702411	4.387015	31.49868
656	4.259809	3.703615	4.429213	31.553387
657	4.265819	3.704828	4.471462	31.608246
658	4.271834	3.70605	4.513763	31.66326
659	4.277856	3.707282	4.556118	31.718435
660	4.283885	3.708523	4.598528	31.773777
661	4.289922	3.709775	4.640996	31.82929
662	4.295966	3.711038	4.683522	31.884979
663	4.302018	3.71231	4.72611	31.940849
664	4.308078	3.713594	4.768762	31.996906

665	4.314148	3.714888	4.81148	32.053154
666	4.320227	3.716193	4.854268	32.109596
667	4.326315	3.71751	4.897128	32.166241
668	4.332415	3.718837	4.940064	32.223091
669	4.338524	3.720177	4.983078	32.280155
670	4.344646	3.721528	5.026176	32.337437
671	4.350778	3.72289	5.06936	32.394939
672	4.356924	3.724264	5.112635	32.452671
673	4.363081	3.725651	5.156005	32.510632
674	4.369253	3.727049	5.199474	32.568836
675	4.375438	3.728459	5.243047	32.627277
676	4.381637	3.729881	5.286729	32.68597
677	4.387852	3.731316	5.330525	32.744919
678	4.394082	3.732762	5.374441	32.804123
679	4.400328	3.734221	5.418481	32.86359
680	4.406591	3.735692	5.462652	32.923328
681	4.412871	3.737174	5.50696	32.983337
682	4.419169	3.738669	5.551411	33.043625
683	4.425486	3.740176	5.596011	33.104195
684	4.431822	3.741695	5.640766	33.165054
685	4.438178	3.743226	5.685685	33.226204
686	4.444554	3.744768	5.730772	33.287651
687	4.450952	3.746322	5.776038	33.349396
688	4.45737	3.747888	5.821487	33.411449
689	4.463812	3.749465	5.867128	33.473812
690	4.470276	3.751053	5.91297	33.536484
691	4.476764	3.752652	5.959019	33.599476
692	4.483276	3.754262	6.005284	33.662788
693	4.489814	3.755882	6.051775	33.726425
694	4.496377	3.757513	6.098498	33.790386
695	4.502966	3.759154	6.145463	33.854683
696	4.509582	3.760804	6.19268	33.919312
697	4.516226	3.762464	6.240157	33.984276
698	4.522898	3.764133	6.287904	34.04958
699	4.529599	3.765811	6.33593	34.115227
700	4.536329	3.767498	6.384245	34.181221
701	4.54309	3.769192	6.432859	34.247559
702	4.549882	3.770894	6.481783	34.314247
703	4.556705	3.772604	6.531026	34.381283
704	4.563561	3.77432	6.580598	34.448673

705	4.570449	3.776042	6.630512	34.516415
706	4.577371	3.777771	6.680776	34.584515
707	4.584327	3.779504	6.731402	34.652966
708	4.591318	3.781243	6.782401	34.721775
709	4.598344	3.782986	6.833784	34.790939
710	4.605406	3.784733	6.885563	34.860462
711	4.612505	3.786483	6.937748	34.93034
712	4.619641	3.788236	6.990352	35.000576
713	4.626815	3.78999	7.043386	35.071167
714	4.634027	3.791747	7.096861	35.142113
715	4.641278	3.793504	7.15079	35.213409
716	4.648569	3.795261	7.205185	35.285061
717	4.655899	3.797017	7.260057	35.357059
718	4.66327	3.798773	7.315419	35.429409
719	4.670683	3.800526	7.371282	35.502106
720	4.678137	3.802277	7.42766	35.575146
721	4.685634	3.804024	7.484564	35.648525
722	4.693172	3.805767	7.542007	35.72224
723	4.700755	3.807505	7.600001	35.796295
724	4.708381	3.809237	7.658559	35.870674
725	4.71605	3.810963	7.717693	35.945385
726	4.723764	3.812681	7.777417	36.020416
727	4.731524	3.814391	7.837741	36.095764
728	4.739328	3.816092	7.898679	36.171421
729	4.747179	3.817782	7.960244	36.247391
730	4.755075	3.819462	8.022449	36.323658
731	4.763018	3.82113	8.085304	36.400219
732	4.771008	3.822785	8.148824	36.477074
733	4.779044	3.824427	8.21302	36.554207
734	4.787128	3.826054	8.277906	36.631618
735	4.795259	3.827665	8.343494	36.709297
736	4.803439	3.82926	8.409797	36.787235
737	4.811667	3.830837	8.476825	36.865425
738	4.819943	3.832396	8.544591	36.943863
739	4.828268	3.833935	8.613109	37.022533
740	4.836641	3.835454	8.68239	37.101433
741	4.845064	3.836951	8.752445	37.180546
742	4.853535	3.838426	8.823288	37.259869
743	4.862056	3.839877	8.894929	37.33939
744	4.870625	3.841303	8.967381	37.419098

745	4.879245	3.842704	9.040654	37.498985
746	4.887913	3.844078	9.114761	37.579037
747	4.896631	3.845424	9.189713	37.659241
748	4.905398	3.846741	9.265519	37.73959
749	4.914215	3.848028	9.342193	37.820068
750	4.923081	3.849283	9.419743	37.900669
751	4.931996	3.850507	9.498181	37.981373
752	4.94096	3.851697	9.577518	38.062172
753	4.949974	3.852854	9.657763	38.143051
754	4.959036	3.853974	9.738926	38.223995
755	4.968147	3.855058	9.821017	38.304993
756	4.977307	3.856104	9.904045	38.386028
757	4.986515	3.857111	9.988021	38.467087
758	4.99577	3.858079	10.072952	38.548157
759	5.005075	3.859005	10.158848	38.629219
760	5.014426	3.85989	10.245716	38.710258
761	5.023824	3.860731	10.333566	38.791264
762	5.033269	3.861528	10.422404	38.872215
763	5.042761	3.862279	10.512239	38.953098
764	5.052299	3.862984	10.603079	39.033897
765	5.061882	3.863641	10.694929	39.114594
766	5.071511	3.86425	10.787797	39.195168
767	5.081184	3.864809	10.881689	39.275608
768	5.090902	3.865316	10.976612	39.355896
769	5.100663	3.865772	11.07257	39.436008
770	5.110468	3.866176	11.169569	39.515934
771	5.120315	3.866525	11.267613	39.595654
772	5.130205	3.866819	11.36671	39.675144
773	5.140135	3.867057	11.46686	39.754391
774	5.150106	3.867238	11.568069	39.833374
775	5.160118	3.867361	11.670341	39.912075
776	5.170169	3.867424	11.773678	39.990475
777	5.180259	3.867428	11.878083	40.06855
778	5.190386	3.86737	11.983558	40.14629
779	5.200551	3.86725	12.090105	40.223667
780	5.210752	3.867068	12.197725	40.300667
781	5.220989	3.866821	12.30642	40.377266
782	5.231261	3.86651	12.416191	40.453445
783	5.241567	3.866133	12.527037	40.529182
784	5.251905	3.865689	12.638957	40.604465

785	5.262276	3.865178	12.751951	40.679264
786	5.272678	3.864598	12.866018	40.753563
787	5.283111	3.863949	12.981157	40.827339
788	5.293572	3.86323	13.097365	40.900574
789	5.304063	3.86244	13.214641	40.973248
790	5.31458	3.861578	13.332978	41.045338
791	5.325125	3.860645	13.452377	41.116825
792	5.335694	3.859637	13.572832	41.187691
793	5.346288	3.858557	13.694339	41.257908
794	5.356905	3.857401	13.816893	41.327461
795	5.367545	3.85617	13.940488	41.396332
796	5.378205	3.854863	14.065119	41.464493
797	5.388885	3.85348	14.190779	41.531925
798	5.399585	3.85202	14.317462	41.598614
799	5.410302	3.850481	14.445161	41.664536
800	5.421036	3.848865	14.573867	41.729668
801	5.431785	3.847169	14.703573	41.793991
802	5.442548	3.845394	14.83427	41.857487
803	5.453324	3.84354	14.965948	41.920135
804	5.464112	3.841604	15.098599	41.981918
805	5.474911	3.839588	15.232212	42.042812
806	5.485719	3.837491	15.366776	42.102798
807	5.496535	3.835312	15.502282	42.161861
808	5.507359	3.833051	15.638717	42.219978
809	5.518188	3.830708	15.776069	42.27713
810	5.529021	3.828282	15.914326	42.333302
811	5.539857	3.825773	16.053474	42.38847
812	5.550695	3.823181	16.193504	42.442623
813	5.561534	3.820505	16.334398	42.495739
814	5.572372	3.817746	16.476143	42.547798
815	5.583208	3.814903	16.618727	42.598785
816	5.59404	3.811975	16.762131	42.648685
817	5.604868	3.808964	16.906343	42.697479
818	5.61569	3.805868	17.051348	42.745152
819	5.626505	3.802688	17.197126	42.791683
820	5.637311	3.799423	17.343664	42.837063
821	5.648108	3.796074	17.490946	42.881275
822	5.658893	3.792641	17.63895	42.924297
823	5.669666	3.789123	17.787663	42.966122
824	5.680425	3.785521	17.937067	43.006733

825	5.691169	3.781834	18.087141	43.046116
826	5.701897	3.778064	18.237867	43.084259
827	5.712607	3.774209	18.389231	43.121147
828	5.723299	3.77027	18.541206	43.156765
829	5.733969	3.766248	18.693781	43.191101
830	5.744619	3.762142	18.84693	43.224148
831	5.755246	3.757954	19.000635	43.25589
832	5.765848	3.753682	19.154877	43.28632
833	5.776425	3.749327	19.309635	43.315418
834	5.786976	3.744891	19.464888	43.343185
835	5.797499	3.740372	19.620613	43.369606
836	5.807993	3.735771	19.776793	43.394669
837	5.818457	3.73109	19.933405	43.418369
838	5.828888	3.726327	20.090425	43.440697
839	5.839288	3.721485	20.247837	43.461643
840	5.849654	3.716562	20.405613	43.481201
841	5.859984	3.71156	20.563736	43.499367
842	5.870278	3.706479	20.722179	43.516129
843	5.880535	3.70132	20.880926	43.531483
844	5.890753	3.696083	21.039949	43.545422
845	5.900932	3.690768	21.199228	43.557945
846	5.91107	3.685377	21.358742	43.569042
847	5.921166	3.67991	21.518465	43.578716
848	5.931219	3.674368	21.678377	43.586956
849	5.941227	3.668751	21.838455	43.593765
850	5.951191	3.663059	21.998674	43.599136
851	5.961109	3.657295	22.159016	43.603069
852	5.97098	3.651458	22.319454	43.60556
853	5.980802	3.645549	22.479965	43.606609
854	5.990575	3.639569	22.640532	43.606216
855	6.000298	3.633518	22.801125	43.604382
856	6.00997	3.627398	22.961725	43.601105
857	6.01959	3.621209	23.122311	43.596386
858	6.029157	3.614952	23.282858	43.590225
859	6.03867	3.608628	23.443342	43.58263
860	6.048129	3.602238	23.603746	43.573593
861	6.057532	3.595782	23.764044	43.563126
862	6.066878	3.589262	23.924215	43.551228
863	6.076168	3.582678	24.084236	43.537899
864	6.085399	3.576031	24.244087	43.523151

865	6.094572	3.569322	24.403746	43.506981
866	6.103685	3.562553	24.563189	43.489399
867	6.112738	3.555723	24.722397	43.470406
868	6.12173	3.548835	24.881348	43.450012
869	6.13066	3.541888	25.040022	43.428219
870	6.139528	3.534884	25.198397	43.405037
871	6.148333	3.527824	25.356455	43.38047
872	6.157074	3.520709	25.514172	43.354527
873	6.165751	3.513539	25.67153	43.327213
874	6.174363	3.506316	25.828508	43.298542
875	6.18291	3.499042	25.985088	43.268517
876	6.191391	3.491715	26.141249	43.237152
877	6.199806	3.484339	26.296972	43.204449
878	6.208153	3.476913	26.45224	43.170422
879	6.216434	3.46944	26.607033	43.135082
880	6.224646	3.461919	26.761333	43.098434
881	6.23279	3.454352	26.915121	43.060493
882	6.240865	3.446739	27.06838	43.021271
883	6.248871	3.439083	27.221094	42.980774
884	6.256807	3.431384	27.373243	42.939018
885	6.264674	3.423643	27.524813	42.896011
886	6.27247	3.41586	27.675785	42.851768
887	6.280197	3.408038	27.826145	42.806301
888	6.287852	3.400177	27.975876	42.759621
889	6.295436	3.392278	28.124962	42.711742
890	6.302948	3.384342	28.273388	42.662674
891	6.31039	3.376371	28.421141	42.612434
892	6.31776	3.368365	28.568203	42.561035
893	6.325057	3.360324	28.714563	42.508488
894	6.332282	3.352252	28.860205	42.454807
895	6.339435	3.344147	29.005117	42.400009
896	6.346516	3.336012	29.149284	42.344105
897	6.353524	3.327847	29.292696	42.287109
898	6.360459	3.319654	29.435339	42.229042
899	6.367321	3.311432	29.5772	42.16991
900	6.374111	3.303185	29.718267	42.109734
901	6.380828	3.294911	29.85853	42.048523
902	6.387472	3.286613	29.997978	41.986298
903	6.394043	3.278291	30.136599	41.923073
904	6.400542	3.269947	30.274384	41.85886

905	6.406967	3.26158	30.41132	41.793678
906	6.41332	3.253194	30.547401	41.727539
907	6.4196	3.244787	30.682615	41.660461
908	6.425807	3.236361	30.816956	41.592461
909	6.431941	3.227918	30.950413	41.523552
910	6.438003	3.219457	31.082977	41.453747
911	6.443992	3.210981	31.214642	41.383068
912	6.44991	3.202489	31.345398	41.311527
913	6.455755	3.193983	31.475241	41.239143
914	6.461528	3.185464	31.60416	41.165924
915	6.467229	3.176932	31.732151	41.091896
916	6.472858	3.168389	31.859209	41.017071
917	6.478417	3.159835	31.985325	40.94146
918	6.483904	3.151272	32.110493	40.865086
919	6.48932	3.142699	32.234711	40.78796
920	6.494665	3.134119	32.357971	40.710098
921	6.499939	3.125531	32.48027	40.631519
922	6.505144	3.116936	32.601604	40.552238
923	6.510278	3.108336	32.721966	40.472271
924	6.515343	3.099732	32.841354	40.391628
925	6.520338	3.091123	32.959766	40.310333
926	6.525264	3.082511	33.077198	40.228397
927	6.530121	3.073897	33.193645	40.145836
928	6.53491	3.06528	33.309105	40.062664
929	6.53963	3.056664	33.423576	39.978897
930	6.544283	3.048046	33.537056	39.894554
931	6.548868	3.039429	33.649544	39.809647
932	6.553386	3.030814	33.76104	39.72419
933	6.557837	3.022201	33.871536	39.638199
934	6.562222	3.01359	33.981041	39.551689
935	6.566541	3.004982	34.089542	39.46468
936	6.570794	2.996379	34.197052	39.377174
937	6.574982	2.98778	34.303558	39.2892
938	6.579105	2.979187	34.409069	39.20076
939	6.583163	2.970599	34.51358	39.111877
940	6.587158	2.962018	34.617096	39.022564
941	6.591088	2.953445	34.719612	38.932831
942	6.594956	2.944879	34.821133	38.842697
943	6.598761	2.936322	34.921658	38.752171
944	6.602503	2.927773	35.021191	38.661266

945	6.606184	2.919235	35.119728	38.570004
946	6.609802	2.910707	35.217278	38.47839
947	6.61336	2.902189	35.313835	38.38644
948	6.616858	2.893682	35.409409	38.29417
949	6.620295	2.885188	35.503994	38.201588
950	6.623672	2.876706	35.597599	38.108711
951	6.62699	2.868236	35.690224	38.015549
952	6.63025	2.85978	35.781872	37.922115
953	6.633451	2.851338	35.872547	37.828423
954	6.636594	2.84291	35.96225	37.734482
955	6.63968	2.834497	36.050983	37.640308
956	6.64271	2.826099	36.138756	37.54591
957	6.645682	2.817717	36.225567	37.451302
958	6.648599	2.809351	36.311417	37.356495
959	6.651461	2.801001	36.396317	37.261501
960	6.654267	2.792669	36.480267	37.166328
961	6.657019	2.784354	36.563271	37.070992
962	6.659717	2.776057	36.645336	36.975502
963	6.662361	2.767777	36.726463	36.879868
964	6.664952	2.759517	36.806656	36.7841
965	6.667491	2.751275	36.885921	36.68821
966	6.669978	2.743053	36.964264	36.592209
967	6.672413	2.73485	37.041691	36.496105
968	6.674797	2.726668	37.118198	36.39991
969	6.677131	2.718505	37.193802	36.303631
970	6.679414	2.710364	37.268501	36.207283
971	6.681648	2.702243	37.3423	36.11087
972	6.683833	2.694144	37.415207	36.014408
973	6.685968	2.686065	37.487225	35.9179
974	6.688056	2.67801	37.558361	35.821354
975	6.690096	2.669976	37.62862	35.724785
976	6.69209	2.661964	37.698009	35.628201
977	6.694036	2.653975	37.766529	35.531605
978	6.695936	2.646009	37.83419	35.435013
979	6.69779	2.638066	37.900993	35.338425
980	6.699599	2.630147	37.966953	35.241856
981	6.701363	2.622251	38.032066	35.145309
982	6.703083	2.614379	38.09634	35.048798
983	6.704759	2.606531	38.159786	34.952328
984	6.706391	2.598708	38.222404	34.8559

985	6.707981	2.590909	38.284203	34.759533
986	6.709528	2.583134	38.345192	34.663223
987	6.711034	2.575385	38.405369	34.566986
988	6.712498	2.56766	38.464745	34.470825
989	6.713921	2.559961	38.523327	34.374744
990	6.715302	2.552287	38.58112	34.278759
991	6.716645	2.544638	38.63813	34.182865
992	6.717947	2.537016	38.694363	34.087078
993	6.71921	2.529419	38.749828	33.991398
994	6.720435	2.521848	38.804523	33.895832
995	6.721621	2.514303	38.858467	33.800388
996	6.722769	2.506785	38.911655	33.70507
997	6.72388	2.499293	38.964096	33.60989
998	6.724954	2.491827	39.0158	33.514843
999	6.725991	2.484388	39.066772	33.419941
1000	6.726992	2.476975	39.117016	33.325191
1006	6.732265	2.433067	39.403576	32.760098
1012	6.736343	2.390139	39.665558	32.201591
1018	6.739315	2.348203	39.904305	31.650555
1024	6.741261	2.307264	40.12114	31.107738
1030	6.742262	2.267323	40.317348	30.573769
1036	6.742391	2.228375	40.494183	30.049158
1042	6.741718	2.190414	40.652851	29.534313
1048	6.740309	2.153429	40.794506	29.029558
1054	6.738225	2.117407	40.920261	28.535126
1060	6.735523	2.082332	41.03117	28.051186
1066	6.732258	2.048186	41.128235	27.577839
1072	6.72848	2.014953	41.21241	27.115135
1078	6.724235	1.98261	41.284588	26.663074
1084	6.719566	1.951139	41.345623	26.221615
1090	6.714514	1.920517	41.396309	25.790678
1096	6.709115	1.890723	41.437393	25.370157
1102	6.703405	1.861735	41.469585	24.959921
1108	6.697415	1.833529	41.493538	24.559814
1114	6.691175	1.806085	41.509869	24.169662
1120	6.684711	1.77938	41.519157	23.789284
1126	6.678048	1.753392	41.521938	23.418476
1132	6.67121	1.7281	41.518715	23.057037
1138	6.664218	1.703482	41.509956	22.704748
1144	6.657092	1.679517	41.496098	22.361395

1150	6.649849	1.656185	41.477543	22.026756
1156	6.642506	1.633465	41.454674	21.700605
1162	6.635077	1.611339	41.427837	21.382721
1168	6.627578	1.589788	41.397362	21.072882
1174	6.620019	1.568792	41.363548	20.770864
1180	6.612414	1.548334	41.326683	20.476452
1186	6.604773	1.528397	41.287025	20.189425
1192	6.597105	1.508963	41.24482	19.909573
1198	6.589418	1.490017	41.200287	19.636686
1204	6.581723	1.471542	41.153641	19.370564
1210	6.574025	1.453524	41.105072	19.110998
1216	6.566331	1.435946	41.054764	18.857801
1222	6.558648	1.418797	41.00288	18.610779
1228	6.550981	1.402061	40.949574	18.369745
1234	6.543334	1.385725	40.894993	18.13452
1240	6.535714	1.369776	40.839264	17.904928
1246	6.528122	1.354203	40.782513	17.680799
1252	6.520564	1.338992	40.724854	17.461967
1258	6.513042	1.324133	40.666393	17.248272
1264	6.50556	1.309615	40.607224	17.039557
1270	6.49812	1.295426	40.547436	16.835672
1276	6.490725	1.281557	40.487118	16.636473
1282	6.483376	1.267998	40.426342	16.441816
1288	6.476075	1.254739	40.365181	16.251564
1294	6.468824	1.24177	40.303699	16.065588
1300	6.461626	1.229084	40.241959	15.883758
1306	6.454479	1.216671	40.180012	15.705949
1312	6.447386	1.204522	40.117916	15.532043
1318	6.440348	1.192632	40.055714	15.361926
1324	6.433365	1.18099	39.99345	15.195483
1330	6.426438	1.169591	39.931168	15.032609
1336	6.419568	1.158427	39.8689	14.873198
1342	6.412754	1.147491	39.806683	14.71715
1348	6.405998	1.136776	39.744545	14.564366
1354	6.399298	1.126276	39.682522	14.414755
1360	6.392656	1.115986	39.620632	14.268224
1366	6.386072	1.105898	39.558903	14.124685
1372	6.379544	1.096007	39.497353	13.984055
1378	6.373074	1.086308	39.436008	13.84625
1384	6.366661	1.076796	39.374882	13.711191

1390	6.360304	1.067465	39.313992	13.578802
1396	6.354005	1.05831	39.253357	13.44901
1402	6.347761	1.049326	39.192982	13.321741
1408	6.341573	1.040509	39.132889	13.196928
1414	6.33544	1.031854	39.073082	13.074504
1420	6.329363	1.023358	39.013573	12.954403
1426	6.323339	1.015015	38.954369	12.836563
1432	6.31737	1.006821	38.895481	12.720924
1438	6.311455	0.998774	38.836914	12.607428
1444	6.305593	0.990868	38.778675	12.496017
1450	6.299782	0.9831	38.720768	12.386638
1456	6.294024	0.975468	38.6632	12.279236
1462	6.288317	0.967967	38.605968	12.173761
1468	6.28266	0.960593	38.549084	12.070164
1474	6.277054	0.953345	38.492546	11.968395
1480	6.271498	0.946218	38.436356	11.868409
1486	6.26599	0.93921	38.380516	11.770162
1492	6.260531	0.932318	38.325031	11.673608
1498	6.255119	0.925538	38.269894	11.578706
1504	6.249754	0.918869	38.215111	11.485415
1510	6.244436	0.912308	38.160679	11.393695
1516	6.239164	0.905851	38.106598	11.303509
1522	6.233937	0.899497	38.052872	11.214817
1528	6.228754	0.893243	37.999493	11.127586
1534	6.223615	0.887087	37.946461	11.04178
1540	6.21852	0.881027	37.89378	10.957363
1546	6.213467	0.875059	37.841442	10.874304
1552	6.208457	0.869183	37.789452	10.792571
1558	6.203487	0.863396	37.737801	10.712133
1564	6.198559	0.857696	37.686489	10.63296
1570	6.193671	0.852081	37.635517	10.555022
1576	6.188822	0.84655	37.584877	10.478292
1582	6.184013	0.8411	37.534569	10.402741
1588	6.179242	0.835729	37.484589	10.328344
1594	6.174509	0.830436	37.434937	10.255074
1600	6.169813	0.82522	37.385609	10.182905
1606	6.165154	0.820078	37.336601	10.111814
1612	6.160532	0.815009	37.28791	10.041778
1618	6.155944	0.810012	37.239532	9.972772
1624	6.151392	0.805084	37.191463	9.904773

1630	6.146874	0.800225	37.143703	9.837761
1636	6.142391	0.795433	37.096249	9.771714
1642	6.13794	0.790706	37.049095	9.706613
1648	6.133523	0.786044	37.002239	9.642435
1654	6.129138	0.781445	36.955673	9.579163
1660	6.124784	0.776907	36.909401	9.516776
1666	6.120462	0.77243	36.863415	9.455257
1672	6.116171	0.768012	36.817711	9.394588
1678	6.111911	0.763652	36.772289	9.33475
1684	6.10768	0.75935	36.727142	9.275728
1690	6.103478	0.755103	36.68227	9.217505
1696	6.099306	0.75091	36.637665	9.160064
1702	6.095161	0.746772	36.593327	9.103389
1708	6.091045	0.742686	36.549252	9.047465
1714	6.086957	0.738651	36.505436	8.992278
1720	6.082895	0.734668	36.461876	8.937814
1726	6.07886	0.730734	36.418568	8.884056
1732	6.074851	0.726848	36.375507	8.830993
1738	6.070868	0.723011	36.332695	8.77861
1744	6.06691	0.719221	36.290123	8.726894
1750	6.062977	0.715476	36.247791	8.675834
1756	6.059069	0.711777	36.205692	8.625415
1762	6.055185	0.708123	36.163826	8.575626
1768	6.051324	0.704512	36.122189	8.526456
1774	6.047487	0.700943	36.08078	8.477892
1780	6.043673	0.697417	36.039589	8.429924
1786	6.039881	0.693933	35.998619	8.38254
1792	6.036111	0.690488	35.957867	8.33573
1798	6.032363	0.687084	35.917324	8.289482
1804	6.028637	0.683719	35.876991	8.243787
1810	6.024932	0.680392	35.836868	8.198635
1816	6.021247	0.677104	35.796947	8.154016
1822	6.017583	0.673852	35.757225	8.109922
1828	6.013938	0.670637	35.717701	8.066341
1834	6.010314	0.667458	35.678375	8.023266
1840	6.006709	0.664314	35.639236	7.980687
1846	6.003123	0.661206	35.600288	7.938596
1852	5.999555	0.658131	35.561527	7.896984
1858	5.996006	0.65509	35.522945	7.855843
1864	5.992475	0.652081	35.484547	7.815164

1870	5.988962	0.649106	35.446327	7.774941
1876	5.985466	0.646162	35.408279	7.735165
1882	5.981987	0.64325	35.370407	7.695828
1888	5.978526	0.640369	35.332703	7.656924
1894	5.975081	0.637518	35.295162	7.618445
1900	5.971652	0.634697	35.25779	7.580384
1906	5.968239	0.631906	35.220577	7.542735
1912	5.964842	0.629144	35.183525	7.505489
1918	5.961461	0.62641	35.146626	7.468641
1924	5.958095	0.623705	35.109886	7.432184
1930	5.954743	0.621027	35.073296	7.396112
1936	5.951406	0.618376	35.036854	7.36042
1942	5.948084	0.615753	35.000557	7.325099
1948	5.944777	0.613156	34.964409	7.290145
1954	5.941483	0.610584	34.928402	7.255553
1960	5.938202	0.608039	34.892532	7.221315
1966	5.934935	0.605519	34.856804	7.187428
1972	5.931682	0.603023	34.821209	7.153884
1978	5.928441	0.600552	34.785748	7.120679
1984	5.925213	0.598106	34.750416	7.087808
1990	5.921998	0.595683	34.715214	7.055265
1996	5.918794	0.593283	34.680141	7.023046
2002	5.915603	0.590907	34.645191	6.991145
2008	5.912424	0.588554	34.610363	6.959558
2014	5.909256	0.586223	34.575657	6.92828
2020	5.906101	0.583914	34.541069	6.897306
2026	5.902956	0.581627	34.506596	6.866632
2032	5.899822	0.579361	34.47224	6.836254
2038	5.896699	0.577117	34.437996	6.806166
2044	5.893587	0.574893	34.403862	6.776365
2050	5.890485	0.57269	34.369839	6.746847
2056	5.887393	0.570508	34.335922	6.717607
2062	5.884312	0.568345	34.302113	6.688642
2068	5.88124	0.566203	34.268402	6.659947
2074	5.878179	0.564079	34.234798	6.631519
2080	5.875126	0.561975	34.20129	6.603354
2086	5.872083	0.55989	34.167881	6.575447
2092	5.869049	0.557824	34.134571	6.547796
2098	5.866024	0.555776	34.101353	6.520396
2104	5.863008	0.553747	34.06823	6.493245

2110	5.860001	0.551735	34.035198	6.466339
2116	5.857002	0.549742	34.002254	6.439674
2122	5.854012	0.547765	33.969402	6.413247
2128	5.851029	0.545806	33.936634	6.387055
2134	5.848054	0.543864	33.903954	6.361095
2140	5.845088	0.541939	33.871357	6.335363
2146	5.842129	0.540031	33.83884	6.309856
2152	5.839178	0.538138	33.806404	6.284572
2158	5.836234	0.536263	33.774048	6.259507
2164	5.833297	0.534403	33.741772	6.234658
2170	5.830368	0.532558	33.709568	6.210023
2176	5.827445	0.53073	33.677441	6.185598
2182	5.824529	0.528917	33.645386	6.161382
2188	5.82162	0.527119	33.613407	6.137371
2194	5.818717	0.525336	33.581493	6.113562
2200	5.815821	0.523568	33.549652	6.089952
2206	5.812932	0.521814	33.517879	6.066541
2212	5.810048	0.520075	33.486176	6.043324
2218	5.80717	0.518351	33.454533	6.020299
2224	5.804298	0.51664	33.422958	5.997464
2230	5.801432	0.514943	33.391441	5.974816
2236	5.798571	0.51326	33.359993	5.952353
2242	5.795716	0.511591	33.328602	5.930073
2248	5.792866	0.509935	33.297268	5.907974
2254	5.790022	0.508293	33.265995	5.886052
2260	5.787183	0.506663	33.234776	5.864306
2266	5.784348	0.505047	33.203617	5.842734
2272	5.781519	0.503443	33.172508	5.821333
2278	5.778695	0.501852	33.141457	5.800102
2284	5.775875	0.500274	33.110455	5.779038
2290	5.773059	0.498708	33.079506	5.75814
2296	5.770249	0.497154	33.048607	5.737405
2302	5.767442	0.495612	33.017757	5.716831
2308	5.76464	0.494083	32.986958	5.696417
2314	5.761842	0.492565	32.956203	5.67616
2320	5.759048	0.491058	32.925495	5.656059
2326	5.756258	0.489564	32.894833	5.636111
2332	5.753471	0.488081	32.864212	5.616316
2338	5.750689	0.486609	32.833637	5.596671
2344	5.74791	0.485148	32.803101	5.577174

2350	5.745135	0.483698	32.77261	5.557823
2356	5.742362	0.482259	32.742157	5.538618
2362	5.739594	0.480832	32.711742	5.519556
2368	5.736829	0.479414	32.681366	5.500635
2374	5.734066	0.478008	32.651028	5.481854
2380	5.731308	0.476611	32.620728	5.463212
2386	5.728551	0.475225	32.590462	5.444707
2392	5.725798	0.47385	32.56023	5.426336
2398	5.723048	0.472484	32.530033	5.4081
2404	5.7203	0.471129	32.499866	5.389996
2410	5.717555	0.469783	32.469734	5.372022
2416	5.714812	0.468447	32.439632	5.354177
2422	5.712072	0.467121	32.409561	5.336461
2428	5.709334	0.465805	32.37952	5.318871
2434	5.706599	0.464498	32.34951	5.301406
2440	5.703866	0.4632	32.319527	5.284064
2446	5.701134	0.461912	32.28957	5.266845
2452	5.698405	0.460633	32.25964	5.249746
2458	5.695678	0.459363	32.229733	5.232768
2464	5.692953	0.458102	32.199856	5.215907
2470	5.690229	0.45685	32.169998	5.199163
2476	5.687508	0.455607	32.140167	5.182536
2482	5.684788	0.454373	32.110355	5.166023
2488	5.682069	0.453147	32.08057	5.149622
2494	5.679352	0.45193	32.050804	5.133335
2500	5.676637	0.450721	32.021057	5.117158